THESIS FOR THE DEGREE OF LICENTIATE OF ENGINEERING

Low temperature CO oxidation over Pt/CeO_2

Noemi Bosio

CHALMERS

Department of Physics
CHALMERS UNIVERSITY OF TECHNOLOGY
Göteborg, Sweden 2021

Low temperature CO oxidation over Pt/CeO_2

Noemi Bosio

Department of Physics
Chalmers University of Technology
SE-412 96 Göteborg
Telephone +46 31 772 1000

Cover:
Ball model of CO_2 formation on Pt/CeO_2

Typeset in LaTeX using the kaobook class
Printed by Chalmers Digitaltryck
Göteborg, Sweden 2021

Low temperature CO oxidation over Pt/CeO_2

Noemi Bosio
Department of Physics
Chalmers University of Technology

Abstract

The oxidation of CO to CO_2 is a widely studied reaction not only for its practical applications but also for its apparent simplicity. CO oxidation is, in fact, often used as a model reaction for other oxidation reactions. On metal surfaces, the reaction is known to follow a Langmuir-Hinsenlwood mechanism where CO and dissociated O_2 react to form CO_2 that desorbs. Despite the high cost of platinum catalysts, it is hard to match the activity of CO oxidation using other metals. Instead of changing the catalysts, the approach is to reduce the amount of necessary metal to carry out the reaction. In this thesis, density functional theory (DFT) calculations and kinetic Monte Carlo (kMC) simulations are used to investigate the reaction energetics and kinetics on model systems, with a focus on the low temperature regime. Stimulated by the experimental evidence that CO may dissociate at low temperatures, CO dissociation has been studied as a possible initial competing reaction to oxidation. Our results show that CO dissociation does not occur directly, even on stepped surfaces. Instead, we propose that dissociation is facilitated at high coverages by a Boudouard reaction path at undercoordinated sites.
In order to study the reaction kinetics, a complete description of the energy landscape is necessary. To describe the reaction landscape, scaling relations like the Brønsted-Evans-Polanyi and structure sensitive relations that link the adsorption energy of the reactants with a chosen descriptor, can be used to reduce the computational cost. Scaling relations are used in this work together with kinetic Monte Carlo to study CO oxidation over Pt nanoparticles. The sensitivity of the kinetic behaviours on scaling relations and on the oxygen sticking probability is investigated. Our results show that varying the slope of the scaling relations changes the turnover frequency (TOF) of the reaction, but the general behaviour is maintained, and clear trends are established between the reaction kinetics and the slope of the scaling relations.
It is known that reducible oxides like ceria can increase the reaction's activity at low temperatures, by allowing for a Mars-van Krevelen path. In this way, the issue with CO poisoning is reduced. We explore the effect of Mars-van Krevelen reaction steps for CO oxidation over Pt/CeO_2. Additionally, we show that the common experimental assignment of XPS spectra shifts for the O 1s to the formation of oxygen vacancies might need reconsideration. Such shift could instead be due to OH groups adsorbed on the surface.

Keywords: Heterogeneous catalysis, CO oxidation, Cerium oxide, density functional theory, kinetic Monte Carlo

Tom.

List of Publications

This thesis is based on the following appended papers, referred to by Roman numerals in the text:

I. Interplay between CO disproportionation and oxidation: on the origin of the CO reaction onset on atomic layer deposition-grown Pt/ZrO_2 model catalysts

V. Pramhaas, M. Roiaz, N. Bosio, M. Corva, C. Rameshan, E. Vesselli, H. Grönbeck, and G. Rupprechter

ACS Catalysis, 11 **(2021)**, 208-214

II. Sensitivity of Monte Carlo simulations to linear scaling relations

N. Bosio, and H. Grönbeck

The Journal of Physical Chemistry C, 124 **(2020)**, 11952–11959

III. On the signatures of oxygen vacancies in O1s core level shifts

A. Posada-Borbon, N. Bosio, and H. Grönbeck

Surface Science, 705 **(2021)**, 121761

IV. Alternative reaction mechanisms for CO oxidation on Pt/CeO_2

N. Bosio, M. Di, M. Skoglundh, P.-A. Carlsson, and H. Grönbeck

In manuscript

My Contributions to the Publications

Paper I

I was responsible for all the calculations and co-authored the paper accordingly.

Paper II

I was responsible for all the calculations. I wrote the first draft of the paper, which was finalized together with my co-author.

Paper III

I was responsible for the calculations on the CeO_2 part and co-authored the paper accordingly.

Paper IV

I was responsible for all the calculations. I wrote the first draft of the paper, which was finalized together with my co-authors.

Contents

1 Introduction

Automotive exhaust gases formed during combustion contain many environmentally harmful compounds. Unburnt hydrocarbons (HC), carbon monoxide (CO), nitrogen oxides (NO_x), and sulfur oxides (SO_x) are, for example, pollutants released from gasoline engines. Hydrocarbons and CO are mainly a result of incomplete combustion due to oxygen deficiency. Gasoline engines should be operated close to stoichiometric conditions to allow for simultaneous oxidation of CO and HC and reduction NO_x using the three-way catalyst.

Carbon monoxide is an odorless and tasteless gas, which blocks the transport of oxygen from the lungs to the organs. In large amounts, CO can lead to suffocation. Because CO is poisonous, it is important to control the emissions, which is done by oxidation to CO_2. CO oxidation is important not only for the reaction itself, but is included as a step in many reactions, like the oxidation of hydrocarbons (HC) and methane (CH_4). CO_2, which is the product of CO oxidation, is a greenhouse gas, playing a role in the fast climate change [1–3]. Despite the importance of reducing the overall amount of greenhouse gases in the atmosphere, CO_2 is not directly poisonous. One way to globally reduce CO_2 emissions, is to enable CO oxidation at low temperatures, thus making the combustion process more energy efficient. The operating temperature for CO oxidation, is presently $> 150°C$. To reduce some of the pollutants, like NO_x, new engines working at lower temperatures have been developed [4]. The drawback of such systems is, however, that the temperature is not high enough to oxidize CO [5]. In order to reduce CO emissions and to be energy efficient, it is important to investigate the possibility to perform CO oxidation at low temperatures.

1.1 Catalysis

One critical technology for emission control is catalysis. Catalysis is commonly divided into heterogeneous, homogeneous and enzymatic catalysis. Catalysis is heterogeneous when the reactants and the catalyst are in different phases. Homogeneous catalysis refers to the case when the reactants and the catalyst are in the same phase [6]. In enzymatic catalysis, enzymes are used as catalysts in biochemical reactions [7]. A catalyst is a material that is used to accelerate a chemical reaction by providing a more favourable pathway [8]. The catalyst takes part in the reaction, but it is not

consumed. In figure 1.1, a schematic of the difference between a non-catalytic and a catalytic process is shown.

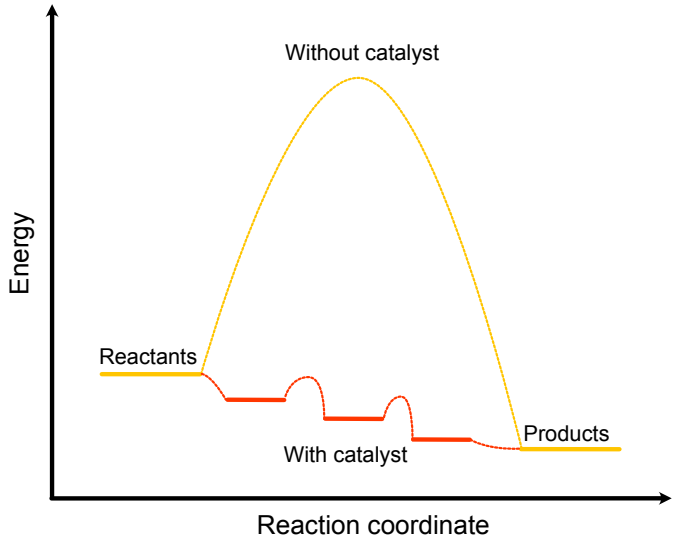

Figure 1.1: Schematic of the energy landscape of a chemical reaction with and without catalyst.

The reaction path created by the addition of the catalyst is more complex, but energetically favourable. The catalyst assembles the reactants, breaks existing bonds, and provides a low energy path to make new bonds. A catalyst is characterized by its activity and selectivity. The activity is the amount of products formed per unit time, while the selectivity is the capacity of the catalyst to drive a reaction towards a certain product. In heterogeneous catalysis, the reaction mechanism will be composed of at least three elementary steps: adsorption, reaction and desorption. The elementary steps form a catalytic cycle. Depending on how the products are formed, different reaction mechanisms can be defined. If one of the reactants adsorbs on the surface, and the other/s react directly from the gas phase, the reaction mechanism is of Eley-Rideal type [9]. When all the reactants adsorb on the surface, the mechanism is of Langmuir-Hinshelwood type. For Langmuir-Hinshelwood reactions, the reactants will diffuse and eventually collide and react. Sometimes the catalyst can take part in the reaction as an atom donor in a, so-called, Mars-van Krevelen mechanism [10]. When the reaction proceeds through this mechanism, one or more atoms from the surface are donated to the reactants.

CO oxidation

Because of the need to remove CO from exhaust gases and for its apparent simplicity [11], CO oxidation to CO_2 is a widely studied reaction. On metal surfaces such as Pt and Pd, the reaction is known to follow a Langmuir-Hinshelwood mechanism [12, 13]. Following this mechanism, the reaction proceeds through a series

of elementary steps, which include the adsorption of CO, the dissociative adsorption of O_2, their reaction and the desorption of CO_2. Despite the limited numbers of elementary steps, the reaction shows fascinating kinetic phenomena such as bi-stability and self-sustained oscillations [14, 15]. In figure 1.2, the bi-stability for CO oxidation is shown.

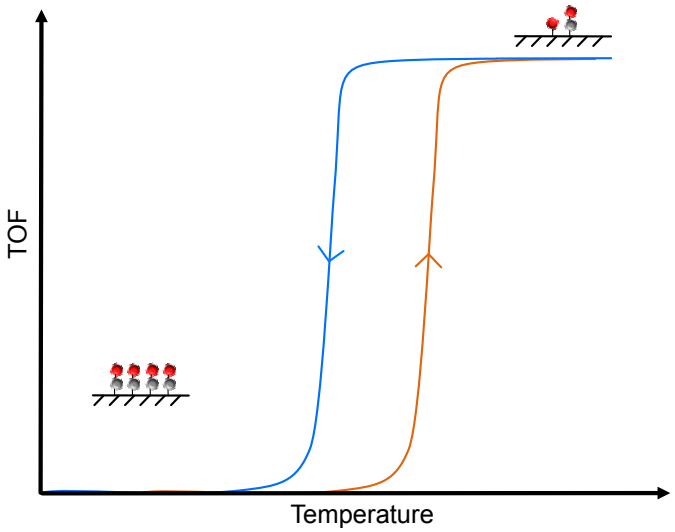

Figure 1.2: Schematic of the bi-stability of CO oxidation. The turnover frequency (TOF) is shown as a function of temperature.

The schematic in 1.2 shows the turnover frequency (TOF) of the reaction as a function of temperature. The reaction shows a hysteresis, meaning that the system is bi-stable. Bi-stability means that depending on the prehistory of the system, the system can be in two different states. One state has a high TOF, whereas the other state has a low TOF. The high activity state is characterized by having both O and CO on the surface, while the low-activity state only has CO on the surface. The main reason for the bi-stability is that CO has a higher adsorption energy than O_2.

Self-sustained oscillations are instead the oscillations in the TOF of the reaction, which can derive from different reasons. One reason is the reduction/oxidation of the metal catalysts due to a variation in reactants pressure [16, 17]. Another reason for oscillations, is structural changes induced by CO adsorption. This may occur on Pt(110) [18]. The Pt(110) surface, reconstructs from a (1x1) to a (1x2) unit cell when the CO coverage is below a critical value. The oscillations originate from the fact that on the restructured (1x2) surface, O_2 hardly dissociates, while oxygen becomes available on the unreconstructed surface. This means that when the system is in the unreconstructed state, oxygen is available and can then react with CO to produce CO_2. A schematic of this phenomena is shown in figure 1.3. When oxygen is available for the reaction, the CO coverage will decrease, eventually leading to the reconstruction of the surface. This less reactive state will be accompanied by an increase in the CO coverage, creating a cycle.

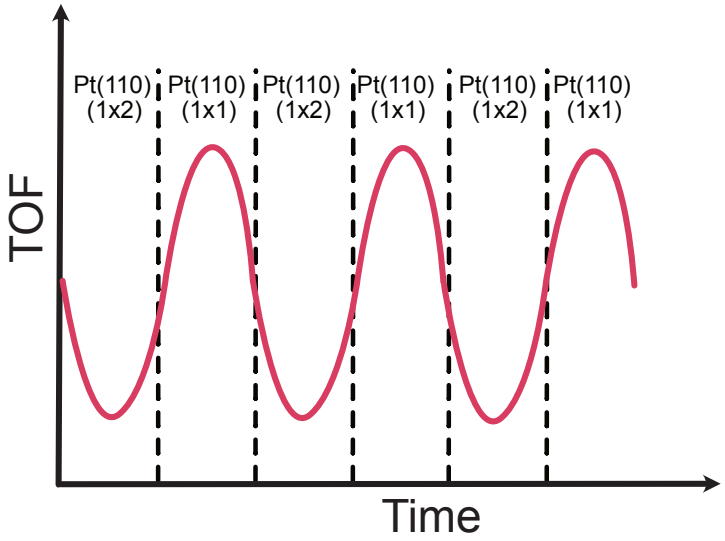

Figure 1.3: Schematic of self-sustained oscillations of the turnover frequency (TOF) for CO oxidation.

To choose a suitable catalyst for a given reaction, one can follow the Sabatier's principle [8]. This principle states that in order to obtain high activity, the reactants should be neither too strongly nor too weakly bound to the catalyst surface. Using this principle, it is possible to predict which catalyst will be the most active for a certain reaction [19]. The catalysts used in the oxidation of CO to CO_2 can be differentiated by the mechanism through which the reaction occurs. Noble metals such as platinum, palladium, and rhodium, are common CO oxidation catalysts with high catalytic activity, sulfur resistance and high resistance to sintering [20, 21]. On noble metals, the reaction is assumed to proceed via the Langmuir-Hinshelwood mechanism with dissociated oxygen. Gold catalysts are used for the oxidation of CO to CO_2 at very low temperatures [22]. On gold catalysts, the reaction proceeds through the Langmuir-Hinshelwood mechanism, but with molecular oxygen. Au catalysts are usually used in air purification systems and in breathing apparatus. Unfortunately, gold can not be used in applications with high temperatures due to the low adsorption energy of the reactants, and rapid sintering. Lastly, several kinds of metal oxide like the metal oxide of Fe, Ni, Mn, Cu, Co and Cr can be used as separate metal oxides or in combination with other metals [23]. Additionally, metal oxides can be used as supports for metal catalysts. Noble metals such as Pd, Pt and Rh have been extensively studied with supports such as cerium oxide, zirconium oxide, alumina, titania and others for the oxidation of CO [24]. Some of these oxides are reducible, and the reaction mechanism is in this case, of Mars-van Krevelen type. One of the extensively studied reducible oxides is ceria (CeO_2). This oxide has been shown to enhance the low-temperature activity of CO oxidation thanks to the possibility of using the oxide lattice oxygen as oxygen reservoir. Experiments have been performed with single atoms catalysts

[25], using nanosized ceria [26], or using metal clusters [27]. The experiments show that single atoms catalysts are not active for the reaction, and that clusters are needed [25]. Furthermore, the use of nanosized ceria gives rise to effects such as oxygen spillover, thus the diffusion of oxygen atoms from the ceria to the metal cluster. Overall, one of the commonly used metals for CO oxidation is platinum. Although platinum is rare and expensive, it is hard to match the activity for CO oxidation. One line of research is presently to reduce the amount of used platinum in the catalyst.

Technological catalysts are usually composed of 1-3 nm particles supported on pourous metal oxides. These systems are structurally complicated and ill-defined. Model experiments are needed to study the catalysts properties. These models usually moves from nanoparticles supported on active oxides, to nanoparticles supported on inert oxides (SiO_2), moving finally to single crystal structures. From the computational perspective instead, a bottom-up perspective is commonly used, studying initially a simple system, and increasing the complexity step by step. The systems studied computationally are well-defined structures where the number of sites is limited. The difference between the systems studied in experiments and computations give rise to the so-called, materials gap [28–30]. With the evolution of technology this gap is closing thanks to the possibility of performing experiments on single nanoparticles [31] and nanoparticles' arrays [32, 33]. Additionally, a so-called pressure gap exists [34]. The pressure gap derives from the difference between the pressures used in experiments, typically ultra-high vacuum, and the pressure experienced in real applications, which are ten orders of magnitude higher. At different pressure, the catalytic system might be different, and is therefore important to study the system at realistic conditions. Experiments at near-ambient pressure and is gradually closing the gap.

As shown schematically in figure 1.2, one of the known problems of CO oxidation on platinum is that at low temperature, the catalyst is CO poisoned, not allowing for the adsorption of oxygen. This means that the reaction can not proceed until the temperature is high enough for CO to desorbs, leaving free sites for oxygen to adsorb. In this thesis, we aim to study CO oxidation over platinum nanoparticles, in order to propose different systems or reaction mechanisms to eventually reduce the CO poisoning problem.

Aim of thesis

The aim of the thesis is to investigate CO oxidation with a particular focus on the low temperature regime. The low temperature regime is of extreme importance due to the fact that in this regime the

reaction is hindered by CO poisoning. In automotive applications this means that during a vehicle cold-start, CO is not oxidized. The cold-start is that period of time between the vehicle is started until it reaches its normal operating temperature. During this time, 90% of pollutants are emitted. The main goal of this thesis is to study CO oxidation over Pt/CeO_2. In order to do so, we first need to understand how CO oxidation proceeds on platinum, how oxygen vacancies are formed on cerium oxide, and what happens when an oxide like ceria is used as support for platinum nanoparticles. At low temperatures, not only CO poisoning is a problem, but it has been proposed that competing reactions might hinder CO oxidation. In paper I, we investigate CO dissociation as a possible competing mechanism to CO oxidation at low temperatures. This is done in collaboration with experimental work. Two different mechanisms for the reaction on different platinum surfaces are studied in terms of density functional theory (DFT) calculations coupled with frequency generation (SFG) spectroscopy and near-ambient pressure X-ray photoelectron spectroscopy (NAP-XPS) to study the dependence of the CO oxidation and the presence of carbon deposits on the surface.

In paper II, the kinetics of CO oxidation is studied over a non-supported platinum nanoparticle. This work is done using kinetic Monte Carlo simulations. Nanoparticles are characterized by a range of different sites. In paper II, scaling relations between the reactants adsorption energy and the generalized coordination number are used to describe the potential energy landscape of the reaction. In particular, we investigated the importance of these relations, and the dependence of the kinetics on the slope of the relations and on the oxygen sticking probability.

In paper III, we investigate the formation of oxygen vacancies in different oxides. Oxides are used as supports, and reducible oxides could, in principle, reduce the problem with CO poisoning allowing the reaction to occur through a different pathway. In paper III, we investigated the O1s core level shifts in oxides. Experimentally, large positive shifts tend to be associated with the formation of oxygen vacancies, however, we propose a different interpretation. In paper IV, we investigate CO oxidation on platinum nanoparticles supported on ceria. DFT and kinetic Monte Carlo simulations are used to study the potential energy landscape and kinetics of the reaction.

The structure of the thesis is that in Chapter 2, a detailed discussion of density functional theory is presented, followed in Chapter 3 by a description of the methods used to calculate some measurable properties. In Chapter 4, a discussion on the method of kinetic Monte Carlo is presented. Chapter 5 focuses on results and lastly, conclusions and outlook are presented in Chapter 6.

Electronic structure calculations 2

> "The underlying physical laws necessary for the mathematical theory of a large part of physics and the whole of chemistry are thus completely known, and the difficulty is only that the exact application of these laws leads to equations much too complicated to be soluble. It therefore becomes desirable that approximate practical methods of applying quantum mechanics should be developed, which can lead to an explanation of the main features of complex atomic systems without too much computation."
>
> Paul Dirac [35]

Dealing with atoms and electrons means that we are treating a quantum many-body problem that can be solved analytically only in the case of one-electron systems such as H. The two main approaches to solve the many-body problem are the Hartree-Fock ansatz and Density functional theory (DFT). This chapter presents an introduction on DFT from theoretical and practical perspectives with emphasis on how DFT can be implemented to find physical and chemical properties of materials.

2.1 Many-body hamiltonian

The total energy of an ensemble of atoms is given by the stationary Schrödinger equation:

$$\hat{\mathcal{H}}\psi = E\psi \tag{2.1}$$

where $\hat{\mathcal{H}}$ represents the Hamiltonian, which contains the energetic operators of the system, E is the energy of the system and ψ is the wavefunction of the system. For a many-body system, the Hamiltonian can be written as:

$$\hat{\mathcal{H}} = \hat{\mathcal{H}}_e + \hat{\mathcal{H}}_n \tag{2.2}$$

which includes the different contributions from N_e electrons and N_Z nuclei. The explicit form of the Hamiltonian [1] is [36]:

$$\begin{aligned}\hat{\mathcal{H}} = -\frac{1}{2}\sum_{i}^{N_e}\nabla_i^2 - \sum_{I}^{N_Z}\frac{1}{2M_I}\nabla_I^2 - \sum_{i,I}^{N_eN_Z}\frac{Z_I}{|r_i - R_I|} \\ + \sum_{i,j>i}^{N_eN_Z}\frac{1}{|r_i - r_j|} + \sum_{I,J>I}^{N_eN_Z}\frac{Z_IZ_J}{|R_I - R_J|}\end{aligned} \tag{2.3}$$

1: Written in atomic units (a.u.). In this unit system, the elementary charge, Planck's constant, Coulomb force constant and the electron mass are set to unity.

The first two terms are the electronic and nuclei kinetic energy, the third term is the electron-nuclei interaction, the fourth term is the electron-electron interaction and the last term is the nuclei-nuclei interaction.

2.2 Born-Oppenheimer approximation

One common approximation made to simplify the many-body problem is the Born-Oppenheimer approximation, which invokes the adiabatic approximation. The adiabatic approximation implies that a system remains in its eigenstate if a perturbation is acting on it slowly enough. In the case of the electronic problem, the mass ratio between electron and nuclei is so small [2] that the electrons move much faster than the nuclei and adapt instantly to the nuclei movements [37]. When the Born-Oppenheimer approximation is applied to the many-body system, the many-body wavefunction can be separated into an electronic component and a nuclei component as:

2: The mass of a proton is 1836 times that of an electron.

$$\psi_{total} = \psi_{electronic}\psi_{nuclear} \tag{2.4}$$

The electronic hamiltionian is:

$$\hat{\mathcal{H}}_e = \hat{\mathcal{T}}_e + \hat{\mathcal{V}_{ext}} + \hat{\mathcal{V}_{ee}} \tag{2.5}$$

These terms represent the electronic kinetic energy, the nuclei-electron Coulomb interaction and the electron-electron interaction, respectively. The dimensionality of the Schrödinger equation is proportional to the number of electrons. Despite the Born-Oppenheimer approximation, the Schrödinger equation is still a many body-system,which, due to the electron-electron interaction, cannot be solved analytically for many-electrons systems.

2.3 Density functional theory

Different methods have been developed to solve the many-electron problem. One of the first methods was the Hartree-Fock approach [38, 39], which dates back to the 1920s. The Hartree-Fock approach assumes that the many-body wave equation can be approximated by a Slater determinant, which is needed to satisfy the requirement that the wavefunction should be anti-symmetric with respect to exchange of two coordinates [40]. Applying the variational principle to the Slater determinant, allow us to find a set of N-coupled equations for the N spin orbitals.
In 1964, the basis for density functional theory (DFT) was presented by Hohenberg and Kohn. Density functional theory has its roots in the Thomas-Fermi method [41, 42], which is based on the electronic

density instead of the many-body wave function. The idea of DFT is that the ground state energy of a system can be expressed as a functional of the electronic density of the system. Thus, the energy of the system can be described by the electronic density.

Total energy from electronic density

Hohenberg and Kohn formulated the two theorems on which DFT is based [43]. The first theorem states that for any system of electrons moving in an external potential V_{ext}, the energy of the system is uniquely determined by the external potential V_{ext}.

$$E[n(r)] = \int V_{ext}(r)n(r)dr + F[n(r)] \tag{2.6}$$

The second theorem states that the ground state energy of the system is determined by the ground electronic density. Thus, the overall minimum of equation 2.6. Using the electron density, [3] reduces the dimensionality of the system from N electrons positions to three spatial positions. If we separates the contributions from the classical Coulomb repulsion in F[n(r)], the functional can be written as:

3: The electron density is defined as $n(r) = |\Psi|^2$.

$$F[n(r)] = \frac{1}{2}\int\int \frac{n(r)n(r')}{|r-r'|}drdr' + G[n(r)] \tag{2.7}$$

In this way, the total energy can be written as:

$$E[n(r)] = \int V_{ext}(r)n(r)dr + \frac{1}{2}\int\int \frac{n(r)n(r')}{|r-r'|} + G[n(r)] \tag{2.8}$$

where G[n(r)] is a functional which includes the kinetic energy and the quantum mechanics effects. DFT is a correct quantum mechanical approach to the many-body problem, however, the actual form of the functional G[n(r)] is unknown.

The Kohn-Sham approximation

What has made DFT usable is the Kohn-Sham approach to the Hohenberg-Kohn result [44]. In 1965, Kohn and Sham provided an approximation for the G[n(r)] functional. They suggested that the many-body problem can be approached by solving a set of one-electron equations. This means replacing the system of interacting electron with a system of non-interacting electrons. The Kohn-Sham ansatz allows for a proper description of the kinetic energy term, which can be separated from G[n(r)]:

$$G[n(r)] = T_{non\_int}[n(r)] + E_{xc}[n(r)] \tag{2.9}$$

This is important since the kinetic energy of the system constitutes a main contribution to the total energy. If we denote the one-electron orbitals with ϕ_i, the kinetic energy of the non-interacting electrons is written as:

$$T_{non\_int}[n(r)] = -\frac{1}{2}\sum_i \langle\phi_i|\nabla^2|\phi_i\rangle \tag{2.10}$$

The electron density is given in terms of the one-electron orbitals given by:

$$n(r) = \sum_i \langle\phi_i|\phi_i\rangle \tag{2.11}$$

E_{xc}[n(r)], the exchange-correlation functional, remains as the unknown in the total energy. E_{xc}[n(r)] includes all the quantum mechanical effects and needs to be approximated. The exchange-correlation functional can be written as:

$$E_{xc}[n(r)] = (T[n(r)] - T_{non\_int}[n(r)]) - (V_{int}[(r)] - J[n(r)]) \tag{2.12}$$

The first parenthesis is the difference between the kinetic energy of interacting electrons and the kinetic energy of non interacting electrons. The second parenthesis is the difference between the electron-electron interaction and the classical Coulomb (Hartree, $J[n(r)]$) interaction. In this way, the total energy of the system can be written as:

$$E[n(r)] = \int V_{ext}(r)n(r)dr + \frac{1}{2}\int\int \frac{n(r)n(r')}{|r-r'|} + T_{non\_int}[n(r)] + E_{xc}[n(r)] \tag{2.13}$$

The Hartree term introduces a self-interaction problem, since the electron interacts with a field created by all the electrons, itself included. This error should, in principle, be cancelled by the exchange-correlation term. Minimizing $E[n(r)]$ with respect to the density and fixed number of electrons, gives the energy corresponding to the ground state density. The electron density would be the same as the true many-body electron density if the exact exchange-correlation functional would be known. The minimization of the total energy yields the Kohn-Sham equations:

$$\left[-\frac{1}{2}\nabla^2 + v_{eff}(r)\right]\phi_i = \epsilon_i\phi_i \tag{2.14}$$

Where the potential v_{eff}(r) is given by:

$$v_{eff}(r) = v_{ext}(r) + v_{Hartree}(r) + v_{xc}(r) \tag{2.15}$$

$$v_{xc}(r) = \frac{\delta E_{xc}[n(r)]}{\delta n(r)} \tag{2.16}$$

The self-consistent solution to the Kohn-Sham equations gives the density and the energy of the system, which results in:

$$E = \sum_i \epsilon_i - E_{Hartree} + E_{xc} - \int n(r) v_{xc}(r) dr \tag{2.17}$$

This means that the single-electrons equations are solved iteratively starting from an initial guess for the electron density. The Kohn-Sham eigenvalues do not have a direct physical meaning. This is, however, not true for the eigenvalue corresponding to the highest occupied state, which, as stated by the Janak's theorem, correspond to the negative of the ionization energy, if the exact exchange-correlation functional is used [45]. DFT is an exact theory, given the exact exchange-correlation functional, meaning that, the accuracy of DFT is given by the accuracy of the exchange-correlation functional approximation (provided that the numerics in the implementation is exact).

Exchange-correlation functionals

All the quantum mechanical effects in the description of the many electron system reside in the exchange-correlation functional.

$$E_{xc} = E_x + E_c \tag{2.18}$$

To properly describe the cohesion between atoms, exchange and correlation need to be accounted for. The exchange-correlation should take into account the anti-symmetry of the many-body wavefunction. In addition, it should account for the fact that the motion of the electrons is correlated. There exist many approximations to the exchange-correlation functional. The approximations differ in the way the details of the electron density are accounted for. The order of the approximations can be ordered in the, so-called, Jacob's ladder [46].

Local density approximation

The local density approximation (LDA) was proposed by Kohn and Sham [43]. The exchange-correlation functional is in LDA given by the exchange-correlation functional of a homogeneous electron gas,

$$E_{xc}[n(r)] = \int n(r) \epsilon_{xc}^{hom}[n(r)] dr \tag{2.19}$$

where $\epsilon_{xc}^{hom}[n(r)]$ is the energy per electron in a homogeneous electron gas with density $n(r)$. The LDA formalism is known to underestimate bond lengths, and it is known to overestimate binding energies and to give unreliable activation energies in chemical

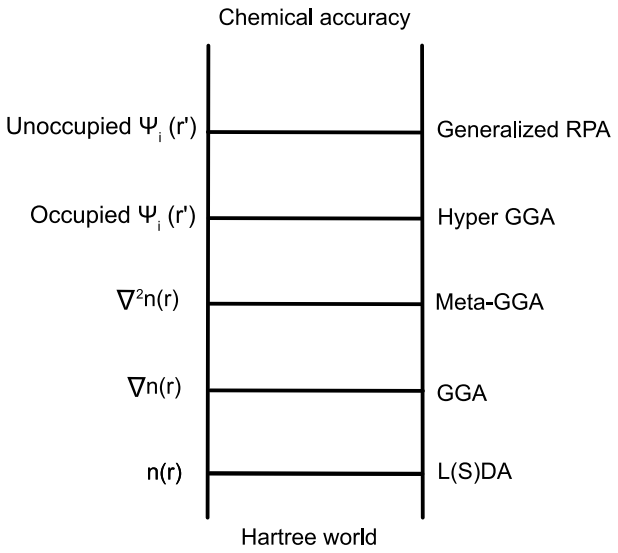

Figure 2.1: Schematic of Jacob's ladder from [46].

reactions. However, it reproduces trends and for some systems lattice constants and cohesive energies are in fair agreement with experiments [47]. Despite its simplicity, LDA works reasonably well, in particular for metals. The good performance is in these cases thanks to an error cancellation deriving from both an underestimation of correlation and an overestimation of exchange [47]. One more fundamental problem of the LDA approximation is the poor description of band gaps. DFT can be generalized for spin polarized systems decomposing the density n(r) into spin-up and spin-down components. In this case, the Kohn-Sham equation needs to be solved for both spin channels.

Generalized gradient approximation

Some of the problems with LDA can be resolved by including an inhomogeneous dependence of the exchange-correlation functional on the gradient of the density. In the generalized gradient approximation (GGA), the functional depends both on the density and its gradient. One example of this class of functionals is the Perdew, Burke and Ernzerhof (PBE) functional [48]. In this type of GGA, the functional is described as:

$$E_{xc}[n(r)] = \int n(r)\epsilon_{xc}^{hom}(n(r))F_{xc}[n(r), \nabla n(r)]dr \qquad (2.20)$$

This functional is designed so that it falls to the LDA approximation in the case of a homogeneous gas. In general, the GGA approximation improves total energies, atomization energies, energy barriers and structural energy differences. Still, GGA lacks a complete cancellation of the self-interaction error and gives an inadequate description of strong correlation effect [49]. This can be a problem

in the calculation of band gaps in insulators and semiconductors as well as HOMO-LUMO separations in molecules.

Beyond the generalized gradient approximation

There exist different methods to reduce the shortcomings of LDA and GGA ; an improvement can be obtained by the, so-called, meta-GGA methods where the functional also depends on the kinetic energy density as $E_{xc}[n(r), \nabla n(r), \nabla^2 n(r)]$ [50]. GGA and meta-GGA functionals still include self-interaction contributions. To correct this, there exists self-interaction correction methods (SIC), hybrid functionals, and "+U" methods. In the SIC functionals, the self-interaction is cancelled by making the orbitals feel a Hartree potential which excludes its own charge density [51, 52]. In hybrid functionals, the Hartree-Fock (HF) exchange is included into the functional so that:

$$E_{xc}^{hyb} = \alpha E_x^{HF} + (1-\alpha)E_x^{DFT} + E_c^{DFT} \tag{2.21}$$

The value for α is determined by comparison to experimental data [53]. The increase in accuracy comes at the price of increased computational cost. In the "+U" approach, localization is enforced by adding a potential dependent on the orbital, including a Coulomb repulsive term between strong correlated electrons on the same atom (usually d and f electrons), following the Hubbard method [54]. The strength of the on-site interaction is usually defined by the parameters U and J, which represent the on-site Coulomb repulsion and the on-site exchange, respectively. These parameters can be extracted from ab-initio calculations or obtained by comparison to experimental data. The Hubbard parameter U is defined as:

$$U = E(d^{n+1}) + E(d^{n-1}) - 2E(d^n) \tag{2.22}$$

It represents the Coulomb-energy cost of putting two electrons on the same site. This correction reduces the self-interaction error of partially occupied orbitals and forces the on-site occupancy matrix to either a full or empty state.

Furthermore, GGA does not take into account long range interaction. To do so, van der Waals functionals can be used. In order to include the long term interactions, van der Waals functionals are used [55]. van der Waals forces arise because of induction of a dipole moment from one system to the other. The attraction between these dipole moments results in an interaction. This energy contribution is usually included as a correction to the Kohn-Sham energy.

DFT in practice

The Kohn-Sham orbitals need to be expanded in some basis. Different basis can be used e.g. Gaussians, atomic orbitals or plane waves. In this work, the VASP code [56] has been used, which is a plane wave method. Plane waves are advantageous for periodic systems thanks to their periodicity and the fulfillment of Bloch's theorem. The Bloch's theorem states that the solution of the Schrödinger equation for an electron in a periodic potential can be written as:

$$\phi_k(r) = u_k(r) \exp(i\mathbf{k} \cdot \mathbf{r}) \tag{2.23}$$

where k is the wave number and $u_k(r)$ is a function with the same periodicity as the potential, which means that it can be expressed in terms of Fourier series as:

$$\phi_k(r) = u_k(r) \exp(i\mathbf{k} \cdot \mathbf{r}) = \sum_G C_{k+G} \exp i(\mathbf{k} + \mathbf{G}) \cdot \mathbf{r} \tag{2.24}$$

This means that it is sufficient to describe the electrons in the first Brillouin zone. In principle, one should include all the possible wavenumbers. However, in practice, only some points are included by choosing a cut-off value as:

$$E_{cut} > \frac{1}{2}|k + G|^2 \tag{2.25}$$

This implies that the energy and the density are represented not as integrals but as a sum over special points in the Brillouin zone. When choosing the k-point sampling, a sufficient amount of points needs to be considered so that the Brillouin zone is sufficiently sampled to yield convergence. It is to be noted that for larger cells, fewer k points will be needed because a larger unit cell, results in a smaller Brillouin zone.

Projector augmented waves method

It is typical in electronic structure calculations to assume that the core electrons are frozen. The wave function of the frozen electrons is taken equal to the one of the corresponding gas-phase atom. This approximation arises from the fact that core electrons do not directly take part in the formation of chemical bonds. One difficulty in performing electronic structure calculations is the different nature of the electronic wavefunctions in different regions of space. Usually, the wave function of electrons far from the core is smooth, while for localized electrons in the core, the wave functions show high frequencies oscillations, due to the the number of electrons [4]. Furthermore, the wavefunction could be very peaked close to the core, making its description difficult, using

4: This results from the orthonormality requirement between the valence and core electrons.

plane-waves. The Projector Augmented Waves Method (PAW) is one of the methods that resolve this problem, and it is the method used in this work. This method has been developed by Blöch [57] and divides the wave function into parts; one to describe the core electrons (partial-wave expansion) and one to describe the valence electrons (envelope function). The goal is to find a linear transformation ($\hat{T}$) that starting from an auxiliary wave function ($\tilde{\psi}_n$) can give the true all electron Kohn-Sham wave function (ψ_n):

$$|\phi_n\rangle = \hat{T}\,|\tilde{\phi}_n\rangle \tag{2.26}$$

In this case, n is the quantum number. This leads to a new Kohn-Sham equation to be solved as:

$$\hat{T}^{\dagger}\hat{H}_e\hat{T} = \epsilon_i\hat{T}^{\dagger}\hat{T}\,|\tilde{\phi}_n\rangle \tag{2.27}$$

A proper operator for the transformation should be chosen. The wave function at a certain distance from the core is already smooth, so $\hat{T}$ should only change the wave function close to the nucleus. In this way, the true wave functions can be described in terms of the auxiliary wave function as a linear combination:

$$|\phi\rangle = |\tilde{\psi}\rangle + \sum_i \left(|\tilde{\psi}\rangle - |\tilde{\psi}\rangle\right)\langle\tilde{p}_i|\tilde{\phi}\rangle \tag{2.28}$$

where $|\tilde{\psi}\rangle$ are pseudo wave functions (PS), the initial states, and $|\psi\rangle$ are all-electrons (AE) wave functions, the target functions and $\tilde{p}_i$ is a projector function [57].

Calculating the ground state

The algorithm used to calculate the solutions of the Kohn-Sham equation is schematically shown in figure 2.2. The process starts by guessing the initial electron density. The exchange-correlation potential and the Hartree potential are calculated, and used to calculate the effective potential in equation 2.15. The potential is thereafter used to solve the Kohn-Sham equation. The wave functions are used to calculate the new electron density and the total energy. If a certain criteria for convergence of the energy is reached (usually around 10^{-5} eV), the calculation is considered to be converged, otherwise the process is repeated.

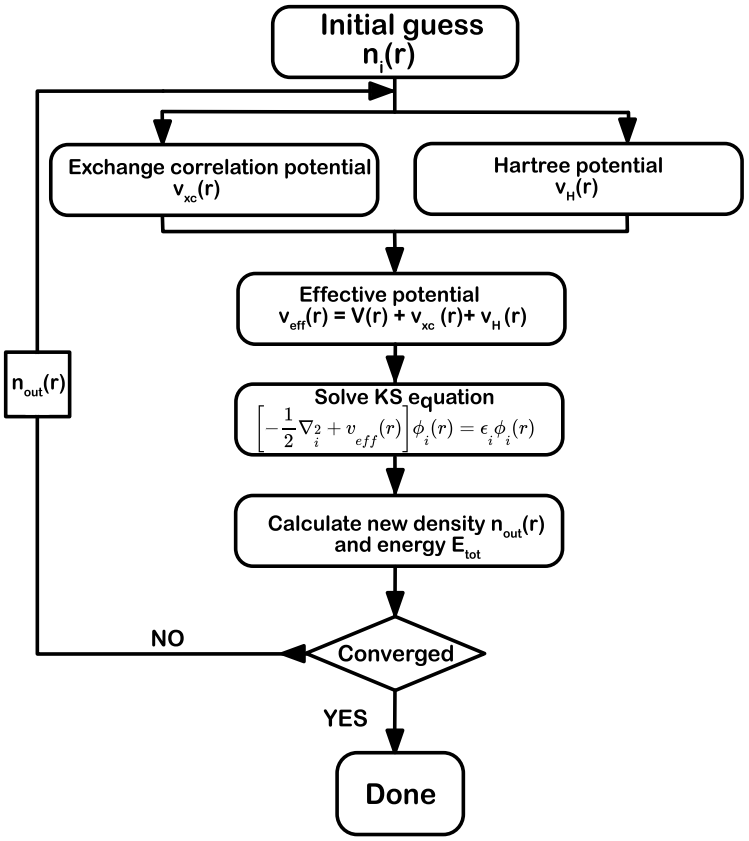

Figure 2.2: Schematic of self-consistency algorithm to find the KS ground state.

From electronic structures to measurable properties

3

In the previous chapter, the theory behind the description of electronic structure was discussed. This chapter elaborates on the details of some methods used to calculate measurable properties from the electronic structure calculations, such as adsorption energies, reaction barriers, vibrational frequencies and core-level shifts.

3.1 Geometry optimization

From statistical mechanics, it is known that the relevant structures are the ones where the system has local minima. The most relevant structure is the ground state, where the energy has its global minima. The minima correspond to a minimum of the energy of the system with respect to the displacement of the nuclei. The geometry optimization corresponds to a minimization of the forces acting on the atoms. In a conservative field, the forces are expressed as the variation of the potential energy, as:

$$f_n = -\frac{\delta E}{\delta R_n} \tag{3.1}$$

The Hellmann-Feynman theorem [58, 59] shows that:

$$-\frac{\delta E}{\delta R_n} = \langle \Psi | \frac{\delta H}{\delta R_n} | \Psi \rangle = \int n(r) \frac{Z_i(r_i - R_n)}{|r_i - R_n|^3} d^3r \tag{3.2}$$

In this case, $n(r)$ is the unperturbed electron density, which means that the forces depend only on the Coulomb interaction between the nuclei and the electron density. The structure is commonly considered to be optimized when the norm of the forces is below a certain value, e.g. $0.01\,\mathrm{eV/Å}$. Many different algorithms have been developed to solve this problem [60]; for example, the RMM-DIIS, conjugate gradient, steepest descent and LBFGS. In this work, the mainly used algorithm is the conjugate gradient method. The method is robust, in particular when the initial guess of the structure is far from the equilibrium structure. In the conjugate gradient method, the first step is a steepest descent step, where the following steps include only conjugate variations. Geometries obtained from these calculations can be compared with experiments where the geometry are obtained, for example, with scanning transmission electron microscope (STEM) [61] or X-ray absorption spectroscopy

(XAS), measuring the Extended X-Ray Absorption Fine Structure (EXAFS) [62].

3.2 Transition states and energy barriers

Other important structural configurations are the transition states. Transition states correspond to the minimum energy barrier, which separates reactants and products during a chemical reaction. These configurations correspond to saddle points between two local energy minima. A saddle point in the potential energy surface is a minimum in all directions except the one which corresponds to the mode along which the reaction occurs.

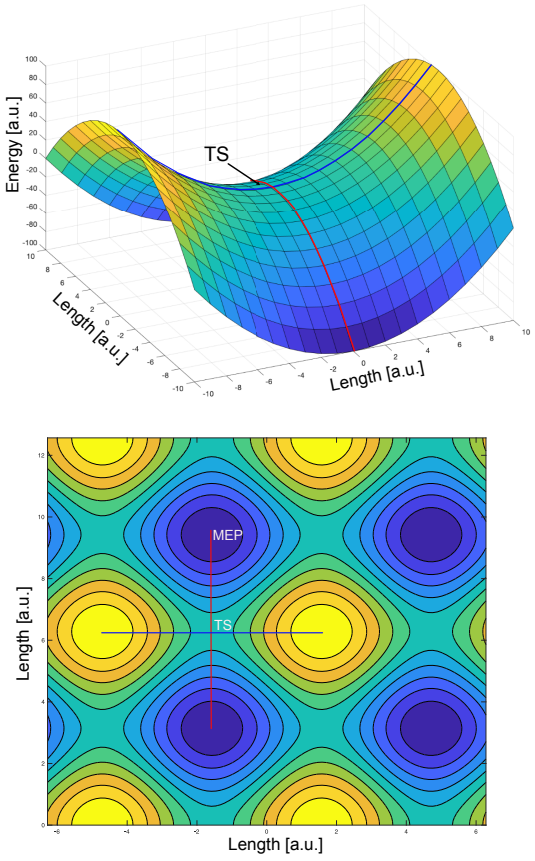

Figure 3.1: Schematic of the potential energy surface (PES) in 3D and 2D. The red line corresponds to the minimum energy path (MEP) and the minimum of the saddle point corresponds to the transition state (TS).

A schematic of the potential energy surface and of the transition state can be seen in figure 3.1. The maxima on the MEP are saddle points in the PES. At the saddle point, the direction of the reaction coordinate is characterized by having a normal mode eigenvector that corresponds to a negative curvature. Different algorithms are used for the search of the transition state as computed to the local minimum. The one used in this work is the, so-called, nudged elastic band method (NEB) [63]. The MEP is in the NEB method

obtained by placing images between the two basins corresponding to the reactants and products configurations. A spring interaction between the images is added in order to maintain continuity. The nudging component means that only normal components of the true force and parallel components of the spring force are included. In this way, the elastic components controls only the spacing between the images. This means that the force on each image is calculated as:

$$F_i = F_i^s|_{\parallel} - \nabla E(R_i)|_{\perp} \tag{3.3}$$

$$\nabla E(R_i)|_{\perp} = \nabla E(R_i) - \nabla E_{R_i}\hat{\tau}_i \tag{3.4}$$

where the second term in equation 3.3 represents the forces that need to be minimized in order to obtain the image's convergence. The spring forces are given by:

$$F_i^s|_{\parallel} = k(|R_{i+1} - R_i| - |(R_i - R_{i-1}|)\hat{\tau}_i \tag{3.5}$$

where $\hat{\tau}_i$ is the normalized tangent at the image i. The energy of the saddle point is calculated by interpolation between these images.

In the case when the barrier is narrow with respect to the length of the MEP, the resolution is poor. In order to avoid this and have a better resolution around the transition state, the NEB method can be modified using the, so-called, climbing nudging elastic band method [63]. In this method, the first iterations are done using the regular NEB algorithm and the image with the highest energy is identified. The image with the highest energy is thereafter released from the spring and the normal force component is maximized to drag to at the top of the band relaxation.

$$F_{imax} = -\nabla E(R_{max}) + 2\Delta E(R_{max})|_{\parallel} \tag{3.6}$$

As the climbing image is not affected by the spring force, the final spacing between the images will be uneven.

3.3 Vibrational frequencies

In order to determine the nature of the points on the potential energy surface, a vibrational analysis can be done. A vibrational analysis gives information on vibrational modes and their corresponding energies (frequencies). These frequencies are commonly calculated in the harmonic approximation, where the forces are calculated as the gradient of the harmonic potential with respect to the atomic displacement. The curvature of the PES is described

by the hessian matrix (Hf), which is calculated as [64]:

$$Hf = \left(\frac{\delta^2 V}{\delta x_i \delta x_j} \right) \tag{3.7}$$

In the harmonic approximation, the energy of each mode is given by:

$$E_i = \hbar \omega_i \left(\frac{1}{2} + n \right) \qquad n = 0, 1, 2, \ldots \tag{3.8}$$

where ω_i are the eigenvalues of the Hessian matrix. The vibrational frequencies can, for example, be used to assure that a suggested transition state is actually a transition state. Knowing that the transition state corresponds to a saddle point, it is known that the curvature of the PES around this point should be positive in all directions except for one. A negative eigenvalue corresponds to a negative curvature, which translates to an imaginary frequency.

The degrees of freedom of a molecule in the gase phase are 3N, where N is the number of atoms. The degrees of freedom describe how the molecule is able to contain and distribute energy. There exists three types of motion, being translational, rotational and vibrational. For non-linear molecules, all rotational motions can be described in terms of rotations around three axes, the rotational degree of freedom are three. As the translational degrees of freedom are 3, the remaining 3N-6 degrees of freedom constitute vibrational motion. For a linear molecule, rotation around its own axis is not a rotation because it leaves the molecule unchanged. Thus, there are only two rotational degrees of freedom for any linear molecule leaving 3N-5 degrees of freedom for vibration. For an isolated molecule, the modes associated with translation and rotation of the entire molecule, will have eigenvalues of zero, while the rest of the vibrations are associated with true vibrations, such as, bond stretches. Calculated molecular vibrations can be compared with experimental measurements usually carried out in terms of infra-red spectroscopy [65].

3.4 Reaction rates

Micro-kinetic modeling and kinetic Monte Carlo simulations represent examples of methods used to study the kinetics of a reaction. In this work, kinetic Monte Carlo methods have been used and will be presented in more detail in chapter 4. In order to use these methods, rates constants need to be calculated, which can be done from first principles using, for example, DFT. The rate constants are commonly estimated using transition state theory (TST) [66, 67]. Transition state theory assumes that for a reaction to take place, the system must lie in a certain region of the phase-space. The initial

and final states are divided by a surface. The points on this surface define the transition state. All the possible transitions from the initial to final state bring the system through the transition state. In figure 3.2, a schematic of a reaction is sketched. The reaction can be written as:

$$R \rightleftharpoons R^{\ddagger} \rightarrow P \tag{3.9}$$

The assumptions of TST are:

- the rate of reaction is low enough so that the Boltzmann distribution is maintained between the initial state (R) and the activated complex ($R^{\ddagger}$).
- the system crosses the diving surface only once, going from reactants to products.

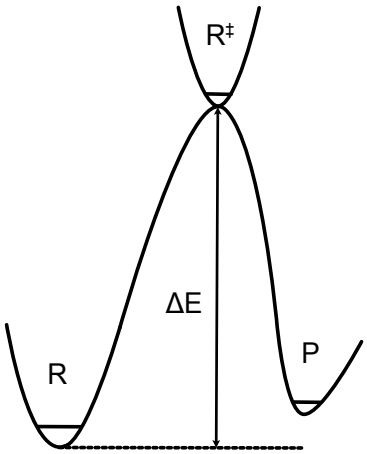

Figure 3.2: Energy profile of reactive system. Adapted from [66].

The second assumption means that the rate constant calculated by TST will always be over estimated. The rate of a reaction is given by the equilibrium number of activated complexes per unit of length normal to and near the top of the potential barrier multiplied by the average velocity of crossing the barrier, thus the TST rate constant is given by [67]:

$$k^{TST} = \nu \frac{Z^{\ddagger}}{Z^{R}} \tag{3.10}$$

where $Z^{\ddagger}$ and Z^{R} are the partition function of the transitions state and of the reactant state respectively, while ν is a frequency of the molecules that pass through the transition state to the final product state (P). This frequency can be calculated by the Maxwell-Boltzmann speed distribution. Considering the case $k_B T >> h\nu$, the rate constant can be expressed as [66]:

$$k^{TST} = \frac{k_B T}{h} \frac{Z^{\ddagger'}}{Z^{R}} \tag{3.11}$$

Where $Z^{\ddagger'}$ is the partition function of the transition state, without the reaction coordinate.

For non-activated adsorption reactions it can be shown that the rate constant is [67]:

$$k_{ads}^{TST} = \frac{pA}{\sqrt{2\pi M k_B T}} \tag{3.12}$$

where p is the gas pressure, A is the area of the adsorption site and M is the mass of the molecule. Given the fact that not all of the molecules that hit the surface stick, a sticking coefficient (s_0) can be introduced, yielding:

$$k_{ads}^{TST} = \frac{s_0 pA}{\sqrt{2\pi M k_B T}} \tag{3.13}$$

The relative desorption rate constant can be determined from the equilibrium constant K, so that:

$$K = \frac{k_{ads}}{k_{des}} = e^{\frac{-\Delta G}{k_B T}} \tag{3.14}$$

where ΔG is the Gibbs free energy change, defined as:

$$\Delta G = \Delta H - T\Delta S \tag{3.15}$$

ΔH and ΔS are the enthalpy and the entropy change, respectively. Calculating the rates through the equilibrium constant makes the reaction thermodynamic consistent.

3.5 Ab-initio thermodynamics

The effects of pressure and temperature on a reaction can be taken into account by the ab-initio thermodynamics formalism [68–70]. Ab-initio thermodynamics allow us to overcome the fact that the results obtained with DFT represent the system at zero Kelvin. The ab-initio thermodynamics approach aims to calculate thermodynamic functions, like the Gibbs free energy, from the results of electronic structure calculations. The approach is based on the idea that a system in equilibrium, can be divided in subsystems, which will be in equilibrium with each other [70]. When a metal is exposed, for example, to O_2 pressure, different structure modifications can occur; from the adsorption on the surface, to the formation of thin film oxides, to the formation of a complete bulk oxide. With ab-initio thermodynamics it is possible, in terms of phase diagrams, to study which of those phases is the most stable under certain temperature and pressure conditions. For a surface, the free energy as a function of temperature and pressure can be

written as:

$$\gamma(T, p_i) = \frac{1}{A}\left[G_{surf} - \sum_i N_i \mu_i(T, p_i)\right] \tag{3.16}$$

where A is the surface area, G_{surf} is the surface free energy, which also depends on temperature and the number of atoms in the sample, μ_i is the chemical potential of the specie i (e.g. O_2) and p_i is the pressure of specie i. The Gibbs free energy is decomposed into different terms:

$$G = E_{tot} + E_{ZPE} + F_{vib} + F_{conf} + pV \tag{3.17}$$

where E_{tot} is the total energy of the system, obtained by DFT, F_{vib} is the vibrational free energy, F_{conf} is the configurational free energy and pV is a pressure volume contribution. The dominant term is the total energy of the system, while the smallest contribution come from the pV term since this contribution will be in the order of [pV/A] = atm $Å^3/Å^2 \simeq 10^{-5}$ eV/$Å^2$. In paper I, ab-initio thermodynamics has been used to calculate the stability of two model systems with respect to the CO coverage. In this case, the chemical potential of CO is calculated as:

$$\mu_{CO}(T, p) = \left[E_{CO} + E_{CO}^{ZPE} + \mu'_{CO}(T, p_0) + k_B T \ln\left(\frac{p_{CO}}{p^0}\right)\right] \tag{3.18}$$

where E_{CO} is the energy of a CO molecule and E_{CO}^{ZPE} is the zero point energy contribution, which has been neglected in this case, $k_B T \ln\left(\frac{p_{CO}}{p^0}\right)$ is the contribution of the CO partial pressure to the chemical potential and μ'_{CO} is the reference chemical potential, calculated from values of enthalpy and entropy taken from thermodynamics tables [71] as:

$$\mu'_{CO} = \Delta H - T\Delta S \tag{3.19}$$

where ΔH and ΔS are defined as the difference between the enthalpy/entropy at the temperature of interest and standard pressure and the enthalpy/entropy at standard temperature and pressure. A reference is needed to study the Gibbs free energy variation in the presence of adsorbates. In Paper I, we used the pristine surface as a reference. Thus, the variation of Gibbs free energy is calculated as:

$$\Delta G_{abs}(T, p) = \frac{1}{A}\left[E_{tot} + N_{ads}(E_{ads} - TS_{vib}^{ads}) - E_{ref} - N_{ads}\mu_{ads}(T, p)\right] \tag{3.20}$$

where E_{tot} is the energy of the system with the adsorbates, E_{ref} is the total energy of the pristine surface, N_{ads} is the number of adsorbed molecules, E_{ads} is the energy of the adsorbate, S_{vib}^{ads} is

the vibrational entropy of the adsorbate and μ_{ads} is the chemical potential of the adsorbate at the desired temperature and pressure. Once the Gibbs free energy variation is calculated, this allows us to understand the state of the system at different conditions. Thus, ab-initio thermodynamics provides a way to link electronic structure calculatios with macroscopic properties.

3.6 Core-level shifts

Core level spectroscopy is one of the techniques used to characterize adsorbates and surfaces experimentally. The technique uses X-rays to measure the binding energy of core electrons [72, 73] and is called X-ray photoelectron spectroscopy (XPS). The idea behind this technique is the photoelectric effect. The surface is irradiated with photons, and electrons are emitted. The exposure of the sample to X-rays creates holes in the core region (core-holes). The kinetic energy of these electrons can be measured as:

$$E_k = h\nu - E_b - \Phi_A \tag{3.21}$$

where E_k is the kinetic energy of the emitted electron, E_b is the binding energy of the electron and Φ_A is the work function of the analyzer. A schematic of the process is shown in figure 3.3. The

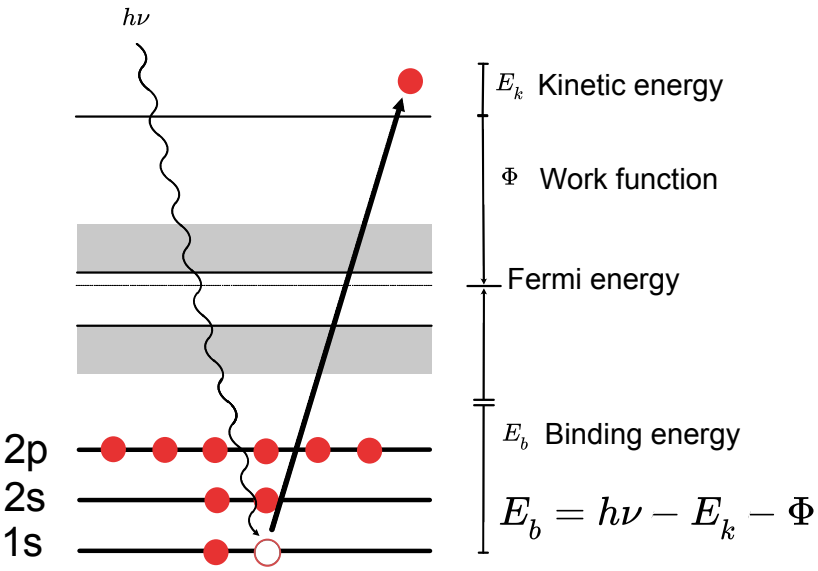

Figure 3.3: XPS schematics for oxygen in an oxide (O^{2-}).

measured photoelectron intensity is directly proportional to the number of photoelectrons. This means that the spectrum can be used to analyze the atomic species present in the sample. With synchrotron radiation, it is possible to distinguish between the binding energy generated from bulk or surface atoms [74].

With DFT it is possible to calculate relative shifts; thus, the dependence of the binding energy on the chemical environment. The

results of these calculations are referred to as core-level shifts (CLS). Experimentally, it can be difficult to assign peaks in the spectrum to a specific specie. Experiments can, thus, be complemented by the computation of CLS for specific species. In the complete screening picture, the core level shifts of surface atoms are calculated as the difference in energy between the system with the core-hole in the reference system (bulk) and the system with the core-hole in the surface. The complete screening approach relies on three assumptions [75].

- The lifetime of the core-hole is longer than the photoelectron emission process.
- The system is in its ground state with the constrain of a core-hole.
- The effect of structural relaxations is small.

With these assumptions, the CLS are calculated as:

$$E_{CLS} = [E^* - E^0] - [E^*_{ref} - E^0_{ref}] \tag{3.22}$$

where E^* and E^*_{ref} are the ground state energy of the system in the presence of a core-hole for the system of interest and the reference system, respectively and E^0 and E^0_{ref} are the ground state energy of the interest and reference system, respectively. There are different approaches to calculate the energies for the ionized system. In the PAW approach, a PAW potential with a core-hole can be generated. This will, however, result in a charged system. This charge can be corrected in two ways; either one electron can be added to the valence band or the cell can be filled with a compensating charge, as an homogeneous jellium background. Adding one electron in the valence band can be problematic for insulators and semiconductors, since it leads to a state in the conduction band. In this work, the CLS for oxides are calculated, and the jellium method is applied [76]. In this case, the calculation of the CLS is reduced to:

$$E_{CLS} = E^* - E^*_{ref} \tag{3.23}$$

An alternative approach to calculate the energy of the ionized system is the, so-called, Z+1 approach, where the ionized atom is substituted with the neighboring specie in the periodic table. Another approximation for the calculation of CLS is the initial state approximation [77]. In this approximation, the CLS are calculated using the Kohn-Sham eigenvalues as:

$$E_{CLS} = [\epsilon_C - \epsilon_f] - [\epsilon^C_{ref} - \epsilon^f_{ref}] \tag{3.24}$$

where ϵ_C and ϵ_f are the eigenvalue of the core-hole of interest and the Fermi energy respectively, while ϵ^C_{ref} and ϵ^f_{ref} are the

eigenvalue of the core-hole and Fermi energy of the reference system.

3.7 Bader charge analysis

One way to study how the surface changes in response to molecular adsorption, is by means of charge transfer analysis. This method can be used to study variations in the oxidation states of atoms, like the change from Ce^{4+} to Ce^{3+} in ceria after the formation of an oxygen vacancy. This method divides the charge of the system in localized volumes where the charge is localized [78]. These volumes are divided by 2-D surfaces (zero-flux surfaces); at a point on these surfaces, the gradient of the charge density has no normal component to the surface, as:

$$\nabla\rho(r) \cdot \hat{\tau} = 0 \tag{3.25}$$

where $\hat{\tau}$ is a unitary vector normal to the surface. As this method is based only on the charge density, it is not sensitive to the basis set used in the calculation of the charge density [78]. Henkelman and coworkers developed an algorithm based on the steepest descent in order to find the maxima in the charge density [79]. This algorithm is grid-based, and the path along the steepest descent is used to define the Bader volumes where the charge is localized. Upon finding the volumes, integration is needed to obtain the total charge in the volume. A schematic of the charge distribution is shown in figure 3.4.

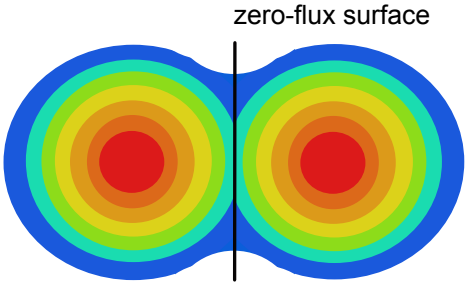

Figure 3.4: Schematic of Bader charge distribution. The black line represents the 2D surface where the density charge has a minimum.

Reaction kinetics 4

This chapter discusses how to simulate and analyze the kinetics of a reaction by means of Monte Carlo methods, using the rate constants calculated in the previous chapter.

4.1 Chemical master equation

The kinetics of a reaction can be seen as the ensemble of transitions between different states of a system. Considering a system of atoms, there is a separation between time scales for reactions and vibrations, which allows for a division of phase space into regions corresponding to different chemical states. Considering two states α and β, the master equation for state α is given by:

$$\frac{dP_\alpha}{dt} = \sum_\beta [W_{\alpha\beta}P_\beta - W_{\beta\alpha}P_\alpha] \tag{4.1}$$

where t is the time, α and β represents different possible configurations of the system, P_α and P_β are the probabilities of the system to be in that particular configuration and $W_{\alpha\beta}$ and $W_{\beta\alpha}$ are transition probabilities per unit time. $W_{\alpha\beta}$ is the transition probability to enter α from β, whereas $W_{\beta\alpha}$ is the transition probability to leave α going to β. The transition probabilities are the rates at which the system changes due to reactions [80]. The master equation describes the time evolution for the probability of observing the system in the different states. The probability of a particular state increases in time, if there is a high transition rate into the state and a low transition state out of the state. Thus, the kinetics will follow the fastest transitions into the most probable states. The master equation can be seen as a gain-loss equation. On the right hand side of equation 4.1, the first term represents an increase for P_α due to processes that change other configurations into α, while the second term represents a decrease in P_α because of processes in α. At equilibrium, the total probability is conserved:

$$\frac{dP_\alpha}{dt} = 0 \tag{4.2}$$

which means that:

$$W_{\alpha\beta}P_\beta(t_0) = W_{\beta\alpha}P_\alpha(t_0) \tag{4.3}$$

where t_0 is the time at which equilibrium has been reached. This equality implies that at equilibrium each process is equilibrated by its reversed process. This is known as the principle of detailed balance [81].

4.2 Kinetic Monte Carlo simulations

Kinetic Monte Carlo (KMC) is a numerical method to solve the master equation. With kinetic Monte Carlo the goal is to be able to consider individual atoms and molecules reacting on a surface, and link this to global changes. Many algorithms have been developed to perform KMC; for example the variable step size method (VSSM), the random selection method (RSM), the first reaction method (FRM) [80]. In this work, the MonteCoffee [82] code has been used, which uses the FRM.

All the KMC methods are used in order to simulate the time evolution of processes of which the rate constants are known, or can be calculated on the fly, meaning that KMC do not predict processes. In order to perform KMC, the elementary steps of the reaction that should be simulated must be known and defined at the beginning of the simulation. Once this is done, the FRM is used. The steps performed by this algorithm are summarized in figure 4.1.

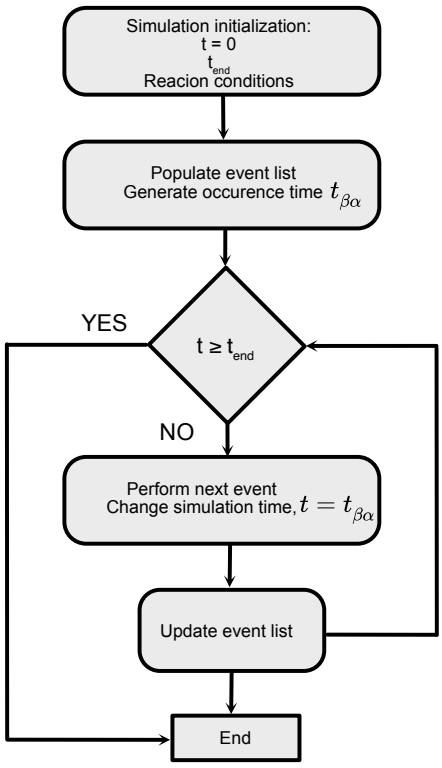

Figure 4.1: Schematic of the First Reaction Method algorithm.

Step 1: In this step, the simulation is initialized choosing an initial time $t = 0$ and a final time t_{end}. The reaction conditions (temperature and pressure) are chosen. A list containing all the possible processes (event list) is created. This list will keep track of the possible events, the site the reaction will take place on and the occurrence time.

Step 2: For each process, an occurrence time is generated as:

$$t_{\beta\alpha} = t - \frac{1}{W_{\beta\alpha}} \ln r \tag{4.4}$$

where $W_{\beta\alpha}$ is the rate constant for the process $\alpha \longrightarrow \beta$ and r is a uniformely distributed random number. The event list is populated at this point.

Step 3: Check if the simulation is ended by checking if $t \geq t_{end}$.

Step 4: The configuration of the system is changed, performing the event with the shortest occurrence time and update the simulation time to the occurrence time of the performed event. Some reactions might be impossible to perform at this step; the reaction is in such cases discarded and the next possible reaction is performed.

Step 5: If the last step executed produced new possible reactions, the event list is updated including those events. In order to save some computational time, this action is performed only in the neighborhood of the site where the last reaction occurred.

Step 6: End of the simulation; all the relevant data is saved.

With this algorithm, the time steps are determined mainly by the reaction rate of the fastest processes, since those will be the events with the highest probability to be executed. In KMC, this is a problem, as the rates of elementary reactions can differ orders of magnitude. The reaction rate of diffusion events, for example, can be orders of magnitudes higher than the ones of chemical reactions. This can make the simulation too computationally costly, since most simulation time will be used to perform the fast events. One of the simplest ideas to solve this problem, is to reduce the rate constant of these processes so that the system will still be brought in equilibrium, but on a shorter time scale. This should be done performing different simulations to find out how much the rate constant should be reduced, for example, by increasing the diffusion barrier. More sophisticated approaches have been developed to tackle this problem. The idea is to find the events which are in equilibrium, and increase the reaction rate constants of these events [83–85]. In Paper II, the simplest approach has been used, increasing the diffusion barrier of CO diffusion.

4.3 Analyzing reaction kinetics

In this section, a discussion about results from KMC simulations and how properties can be obtained is presented.

Coverages and turnover frequency

In order to study the kinetics of a reaction, it is important to monitor which species are present on the surface. Coverage represents the abundance of a specie on the studied system. Coverages can also be compared with experimental measurements, like X-ray photoemission spectroscopy or temperature programmed desorption. Information on the coverage is useful not only for comparison to experiments, but also to understand better the kinetics. Knowing, for example, that during CO oxidation, CO is the abundant specie, means that focusing on a good description of the CO-CO interaction might be more important than focusing on the adsorbate-adsorbate interaction between other species. Moreover, the rate of a reaction is in a mean-field picture proportional to the coverage.

Both the reaction rate and the turnover frequency (TOF) can be used to investigate the speed of a reaction. The reaction rate is the number of products formed per unit of time. The turnover frequency is a measure of the amount of products formed per active site per unit time. When performing kMC simulations, the number of active sites can be defined at the beginning of the simulation. Experimentally, it is usually difficult to know which sites are active or not, so usually the TOF is defined in terms of surface sites. This means that the absolute value of the TOF often differs from the experimental measurements. Nevertheless, the trend does often agree, allowing a qualitative comparison.

Reaction orders

Considering a reaction between reactants A and B, producing the products C and D, the reaction can be written as:

$$\nu_a A + \nu_b B \underset{k^-}{\overset{k^+}{\rightleftharpoons}} \nu_c C + \nu_d D \tag{4.5}$$

where ν are the stoichiometric coefficients, and with forward rate constant k^+ and backward rate constant k^-. The reaction rate is given by [6]:

$$r = -\frac{1}{\nu_a}\frac{d[A]}{dt} = -\frac{1}{\nu_b}\frac{d[B]}{dt} = -\frac{1}{\nu_c}\frac{d[C]}{dt} = -\frac{1}{\nu_d}\frac{d[D]}{dt} \tag{4.6}$$

where $[A]$ is the concentration of the specie A. If the reaction occurs in gas phase, the concentration can be replaced by the standard partial pressure [1]. The total rate can be expressed as a function of the partial pressures [6]:

1: $[X] = \frac{p_X}{p^0}$, p^0=1 bar.

$$r = K p_A^{n_A} p_B^{n_B} p_C^{n_C} p_D^{n_D} \tag{4.7}$$

or more generally:

$$r = K \prod_x p_x^{n_x} \tag{4.8}$$

where K is the equilibrium constant, and n_x are the reaction orders [6]. To obtain reaction orders from KMC, a temperature is chosen, and different simulations are performed varying the partial pressure of the reactant under consideration. The rate is then fitted to this power law. Reaction orders can be compared with experimental measurements.

4.4 Kinetic Monte Carlo simulations in heterogeneous catalysis

In this section, the method of scaling relations Monte Carlo is introduced. Moreover, the dependence of the catalytic activity on the potential energy landscape is discussed, together with the dependence of applied sticking coefficients.

Scaling relations in kinetic modeling

In heterogeneous catalysis, micro-kinetic modelling in combination with scaling relations have been used to study the catalytic reactivity and the design of new catalysts. There exist linear scaling relations for adsorbates bonding on metal surfaces, which relate the energy of one adsorbate to another. Furthermore, relations known as the Brønsted-Evans-Polanyi (BEP) relations [86, 87], relate the activation energy to the adsorbates adsorption energy [88]. For a large number of heterogeneous catalytic reactions, such relations between intermediates and transition states have been identified [89, 90]. This means that the energies of all the reaction intermediates and transition states can be expressed in terms of the energy of a small number of descriptors. DFT can be used to study the electronic structure of catalyst, but it is computationally costly to study each and every possible catalyst. Scaling relations can, thus, provide a tool that can be used to predict the behaviour of numerous catalysts.

By use of scaling relations, the rates can be visualized in terms of volcano plots, where the rate of the reaction are expressed as

a function of the energy of the chosen descriptor. A schematic is shown in figure 4.2. The idea is that plotting the rate of a

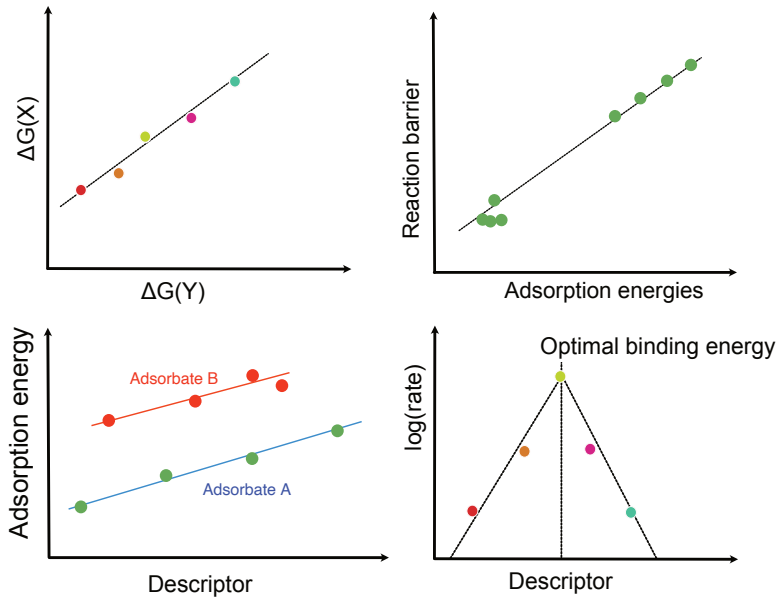

Figure 4.2: Top left: Free energy scaling relation between intermediate x and y. Top right: Brønsted-Evans-Polanyi relation between adsorption energies of reactants and activation barrier. Bottom left: Scaling relations of adsorption energies of specie A and B with respect to the chosen descriptor. Bottom right: Volcano plot resulting from the binding energies. Adapted from [91].

reaction with respect to some adsorption property, then according to Sabatier's principle, the plot will have a maximum, showing the shape like a volcano.

Despite the undeniable utility of such relations, they are not sensitive to the structure of the catalyst. Nanoparticles and stepped surfaces, have different sites which present different reactivity, which gives rise to a structural dependent kinetic. To represent the potential energy landscape of a nanoparticle requires a detailed analysis of a high number of energies. Study these energies by means of DFT calculations would require an incredible amount of computational time. It is then important to find an easier way to obtain those energies. It has been demonstrated that adsorption energies of reactants can be described by means of different descriptors, such as the d-band, the coordination number [92–94] or the generalized coordination number [95]; furthermore also in this case, the relation between the energies and the chosen descriptor results in a linear relation. A schematic is provided on the bottom left of figure 4.2.

Utilizing such descriptors for the binding energies of the reactants, the site-dependent adsorption energy can be studied providing a detailed energy landscape. In this way, it is possible to have a clear picture of the catalyst's activity both on nanoparticles and on surfaces with multiple facets. This approach has been used for example to compare the activity of CO oxidation over Pt(111) and over nanoparticles, where the adsorption energy depend on the adsorption site [95].

4.5 Sensitivity of scaling relations

One question is how sensitive the kinetics of the reaction is to the applied scaling relations. In Paper II, we approached the problem, investigating how the activity of the CO oxidation reaction depends on the slope of the scaling relation and on the oxygen sticking coefficient. The reaction was studied over a platinum nanoparticle. To apply kinetic Monte Carlo, the possible events need to be defined a priori to initialize the simulation. The elementary steps included in the simulations are adsorption and desorption of the reactants, adsorbate diffusion and the formation of CO_2 from adsorbed CO and O. We assume fast desorption of CO_2 once it is formed. The reaction is, thus, modeled as:

$$
\begin{aligned}
CO_{(g)} + * &\leftrightarrow CO* \\
CO* + * &\leftrightarrow * + CO* \\
O_{2(g)} + 2* &\leftrightarrow 2O* \\
O* + * &\leftrightarrow * + O* \\
CO* + O* &\rightarrow CO_{2(g)} + 2*
\end{aligned}
$$

where the subscript (g) represents the molecules in gas phase, whereas $*$ denotes a surface site. In order to describe the different sites present on the nanoparticle, the generalized coordination number (GCN) was used. With respect to the coordination number, the GCN also accounts for coordination of the nearest neighbors and is defined as:

$$
GCN(i) = \sum_{j=1}^{n_i} \frac{CN(j)}{CN_{max}} \tag{4.9}
$$

where CN_j is the coordination number of the atom j. CN_{max} is for platinum 12 and the sum is over the neighbors of the site j. The generalized coordination number for atop sites of the used nanoparticle are shown in figure 4.3.

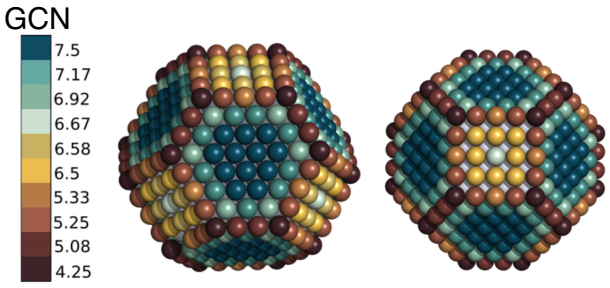

Figure 4.3: Atop sites of an octahedral nanoparticle colored accordingly to the GCN. The particle is composed by 976 atoms.

By comparing simulations where the slope of the scaling relations of the adsorption energy of CO and oxygen is changed, conclusions can be drawn regarding the sensitivity of the kinetic Monte Carlo method. We started comparing the activity for CO oxidation over a nanoparticle and over Pt(111), shown in figure 4.4. The energies used to calculate the rates in figure 4.4 are obtained from DFT calculations..

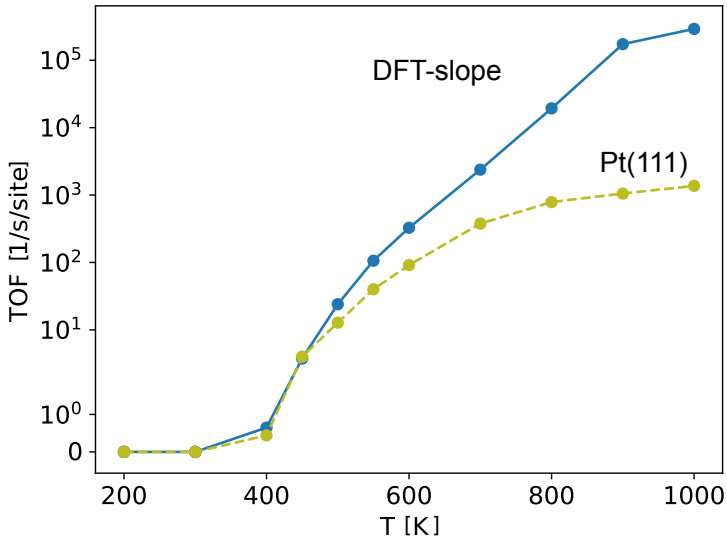

Figure 4.4: TOF as a function of temperature for CO oxidation over a nanoparticle (blue line) and Pt(111) (green line). The DFT energies for these calculations are taken from [95].

The reason for increased activity at high temperatures of nano-sized catalysts with respect to surface ones, is the stronger adsorption energies at low coordinated sites. The presence of different sites also allow to have site specific reactivity. We then changed the slope of the scaling relations, to see how it would affect the kinetics. The results show a small dependence of the light-off temperature on the slope; the light-off temperature slightly increases, increasing the slope, as shown in figure 4.5. The slope has been changed by 40%

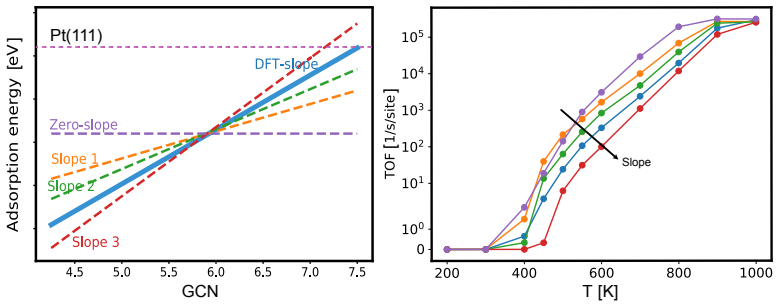

Figure 4.5: Left: Representation of the different slopes of the scaling relations between the adsorption energy and the GCN. The slope for adsorption energy of CO and oxygen has been changed equally. Right: Resulting turnover frequency for each different slope. The DFT-slope represents the scaling relation calculated by DFT from [95].

and the light-off variation between the two limiting cases is about 100 K. The highest TOF is obtained from the case when the slope is flat, meaning that the adsorption energy of both CO and oxygen is the same for all sites on the nanoparticle. This condition is the same

that we would find on a surface. This result might be surprising as it is known that nanoparticles are usually more active than surfaces [96–98]. It should be noticed that in Paper II, the zero slope case, corresponds to an hypothetical surface with an adsorption energy lower than the one that would be found on Pt(111). Roughly, the adsorption energy corresponds to the adsorption energy we would have on the edge sites of a nanoparticle. As stated above, different sites on a nanoparticle are active at different reactions conditions. In figure 4.6, the activity of the different site-types is shown for all the slopes. At low temperatures, the most active sites are edges and

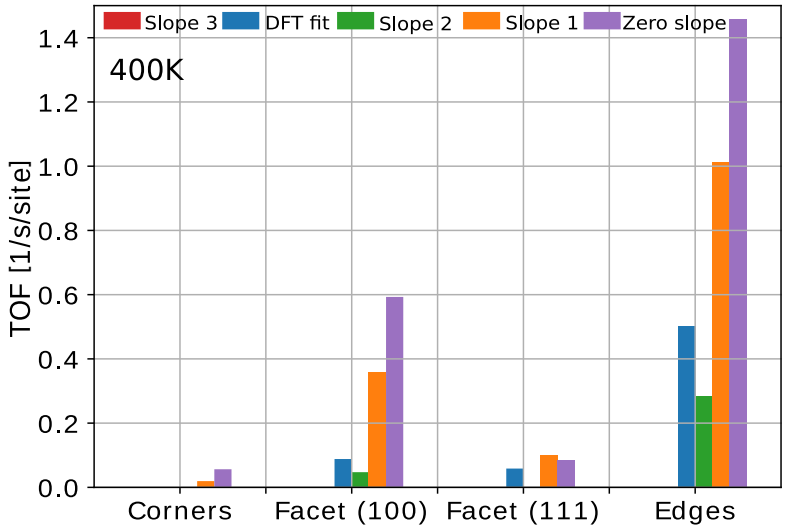

Figure 4.6: Activity for the different slope cases for the different site-type.

the (100) micro-facet. This result agrees with the highest TOF of the zero slope case, where all the sites are edge-like. Interestingly it is found that despite some quantitative change, the trends for the TOF for all the nanoparticles remain the same, and a clear trend between the potential energy landscape and the kinetic is established.

4.6 Sensitivity of scaling relations to the sticking coefficient of oxygen

Another factor that influences the catalytic activity is the sticking coefficient of the reactants. The sticking probability of oxygen, has been measured to have a dependence on the site-type [99–101]. In this case, the dependence of the kinetics on this factor was studied performing calculations where the CO sticking coefficient is kept constant, while the sticking coefficient of oxygen is changed. As shown in figure 4.7, the TOF is not sensitively dependent on the sticking coefficient. In an attempt to analyze the higher TOF when the oxygen sticking coefficient is different on facets and

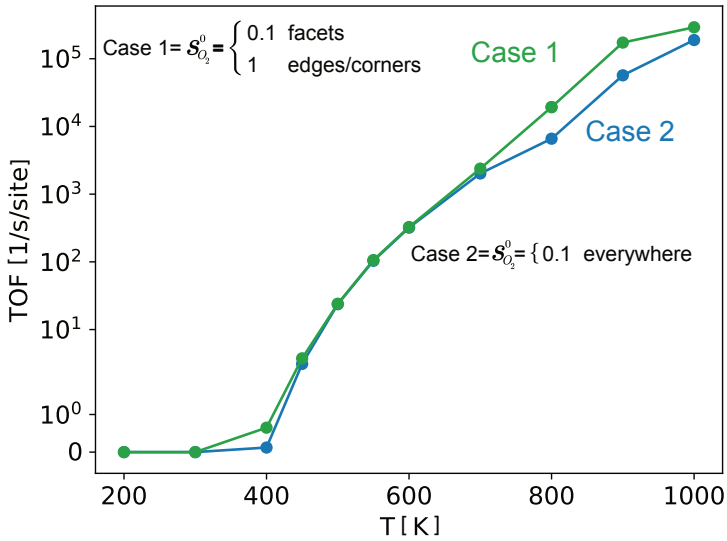

Figure 4.7: TOF as a function of temperature for the different slope cases for the different site-type.

edges/corners, the site activity has been investigated as shown in figure 4.8.

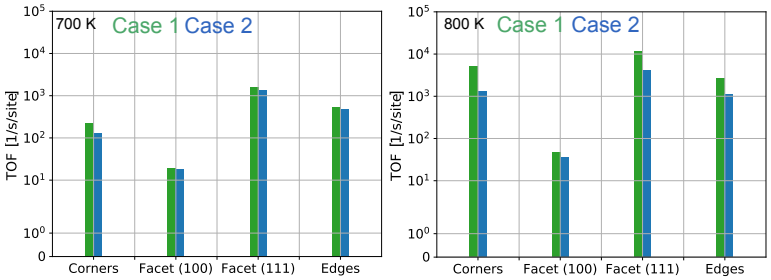

Figure 4.8: Left: Site activity comparison between case 1 and case 2 at 700 K. Right: Site activity comparison between Case 1 and Case 2 at 800 K.

Two temperatures have been chosen, one where the TOF remains the same in both cases (700 K) and one where the TOF is different (800 K). In the case where a higher sticking probability is assigned to edges and corner sites, we observe a higher site activity for all sites. The underlying reason for the increase in the TOF can be found in the oxygen coverage. Overall the reaction kinetics has a small dependence on the sticking coefficient.

Low temperature CO oxidation 5

This chapter will discuss the results related to low temperature CO oxidation. At low temperatures, the activity of CO oxidation is low on platinum catalysts due to CO poisoning. In order for the activity to increase, the coverage of CO should be reduced and alternative reaction paths should be offered. Another problem might be represented by the presence of competing reactions. The main goal is to study CO oxidation on platinum nanoparticles supported on cerium oxide. In order to do so, we break down the reaction on the different components. We first studied CO oxidation on platinum surfaces in order to get an understanding of how the reaction proceeds, and the possible presence of competing reactions. In chapter 4, we presented a study of the kinetics of the reaction on unsupported nanoparticles, which gave an insight into the importance of the presence of different adsorption sites. We then studied ceria as a pristine oxide, in order to understand its properties. We then tried to put the components together investigating CO oxidation over ceria supported platinum cluster. A brief schematic of the methodology is shown in figure 5.1.

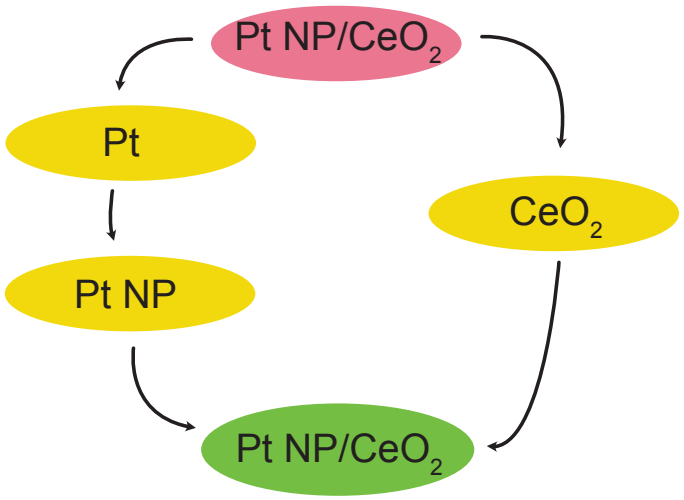

Figure 5.1: Schematic of the systems studied in order to perform CO oxidation on platinum clusters supported on CeO_2.

5.1 CO dissociation over platinum

CO dissociation over platinum has been a puzzling and controversial topic in heterogeneous catalysis, despite some early experimental evidence [102, 103]. In paper I, CO dissociation has been studied computationally over different platinum structures, in order to investigate the conditions at which CO oxidation may

occur. The calculations have been carried out in a collaboration with experimental work.
We started studying CO, carbon and oxygen adsorption on Pt(111), Pt(100). We found that on Pt(111), CO adsorbs preferably in a fcc position, and the same applies for oxygen and carbon. On Pt(100), CO and oxygen prefer to adsorb on bridge sites, while carbon prefers a hollow position.
Initially, we studied, direct dissociation of CO on Pt(111) and Pt(100). As can be seen in figure 5.2, the potential energy landscape results in an endothermic reaction for both surfaces, where the energy difference between a possible final and initial state is around 2 eV. The barriers for CO dissociation was calculated to be 4.5 eV and

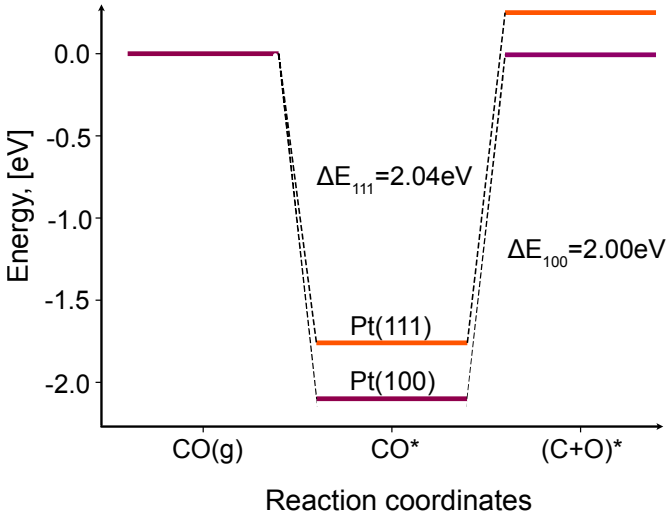

Figure 5.2: Potential energy landscape for CO dissociation over Pt(111) and Pt(100).

3.95 eV for Pt(111) and Pt(100), respectively. Such high barriers imply that CO dissociation can not occur directly on these surfaces at low temperatures. In the literature, it has been suggested that stepped surfaces might facilitate the dissociation [104–106]. We decided to investigate direct dissociation over Pt(211). On Pt(211), CO adsorbs at the four fold site at the step and the same applies to oxygen, while carbon adsorbs in a hcp position. However, also in this case, the reaction is endothermic, and the barrier is higher than 2 eV. The conclusion from these initial calculations are that CO does not dissociate directly over low index Pt-surfaces.
From the energy landscape obtained for Pt(111), Pt(100) and Pt(211), we conclude that the final state of the reaction should be stabilized, and the initial state should be destabilized for the dissociation to occur. To stabilize the final state, the carbon left on the surface after the dissociation has occurred, should occupy a four-fold site and CO_2 should be formed as a reaction product. We suggest a Boudouard-like reaction where two CO molecules react to form CO_2 and carbon as:

$$2CO^* \longrightarrow CO_{2(g)} + C^* \tag{5.1}$$

We believe that for the reaction to proceed, the CO molecules reacting should be arranged in a way so that the π^* orbitals of two adjacent molecules can overlap. A schematic is shown in figure 5.3.

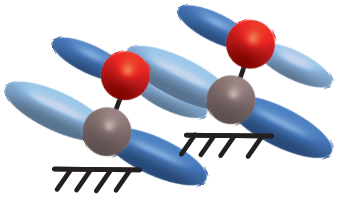

Figure 5.3: Schematic of the interaction between π^* orbitals when the CO molecules are tilted.

Despite this mechanism, the reaction is still endothermic on Pt(211) in the low coverage limit with high barriers. Our conclusion is that neither the kind of surface and the pathway alone can lead to CO dissociation on platinum. In order to lower the barrier, the CO adsorption step should be destabilized further, meaning we need to account for entropy and lateral interactions. For the reaction to occur, particular low-coordinated sites are needed, in parallel with the Boudouard-like path and high CO coverages. These considerations lead us to study CO oxidation over Pt carbonyls and Pt(410).

CO dissociation over ad-atoms

CO adsorption on Pt(100) can lead to surface roughening, which could lead to the formation of special low-coordinated sites for the reaction. The Pt(100) surface has been chosen for the high mobility of surface atoms over this surface [107–109]. Due to the high mobility, single metal atoms could diffuse over the surface and form carbonyl groups. Carbonyls are systems composed of a number of CO molecules adsorbed over a few metal atoms. In our case, we chose a carbonyl composed of two adsorbed CO molecules ($Pt(CO)_2$) on a Pt-adatom. To understand which system would have been the most stable at the experimental conditions, we studied the Gibbs free energy of adsorption. In this way, we can study the stability of the system in dependence of the CO coverage. We find that high coverages of 1 ML and 1.25 ML are possible at the experimental conditions (500 K, 10 mbar). The Gibbs free energy and the chosen structure can be seen in figure 5.4.

At the equilibrium conditions, the reaction proceeds between one CO molecule adsorbed on the Pt adatom, and one CO molecule

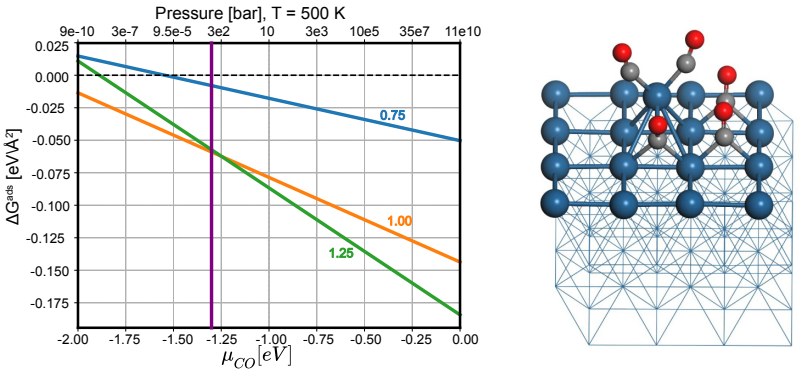

Figure 5.4: Left: Gibbs free energy in dependence of temperature and pressure for different CO coverages for a $Pt(CO)_2$ carbonyl on Pt(100). Right: Structure with relevant coverage of 1.25 ML chosen for the calculations.

adsorbed on the Pt(100) surface below. The barrier for CO dissociation was calculated to be 1.8 eV. In figure 5.5, the structures along the reaction coordinated are shown.

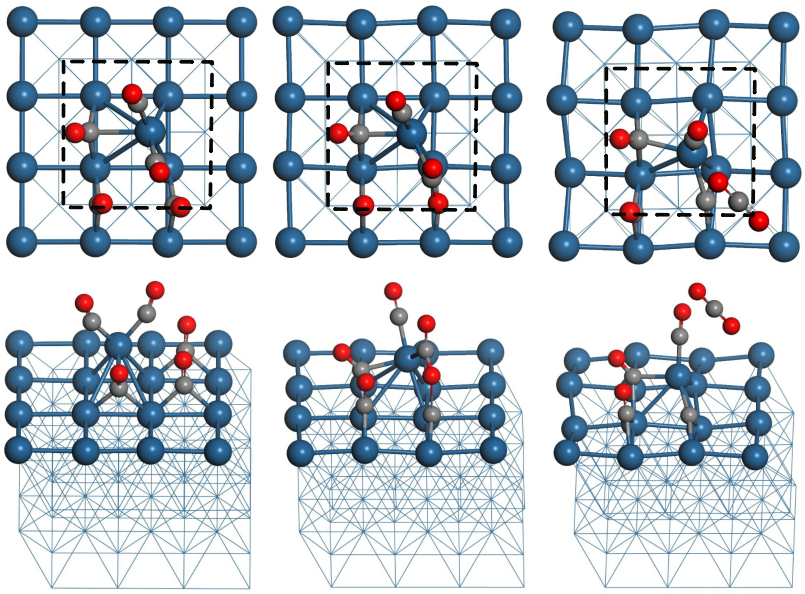

Figure 5.5: Initial (left), transition (middle) and final (right) state for CO dissociation on a $Pt(CO)_2$ over a Pt(100) surface. Top and side view. CO coverage = 1.25 ML.

CO dissociation over Pt(410)

A second possible reaction path was considered over a step of a Pt(410) surface. This surface was chosen as a model system since experimentally, this surface showed high activity for CO dissociation [104]. As for the carbonyl case, we studied the Gibbs free energy of adsorption in order to find the most stable coverage configuration at the used experimental conditions. As can be seen in figure 5.6, the resulting equilibrium coverage is 0.6 ML.

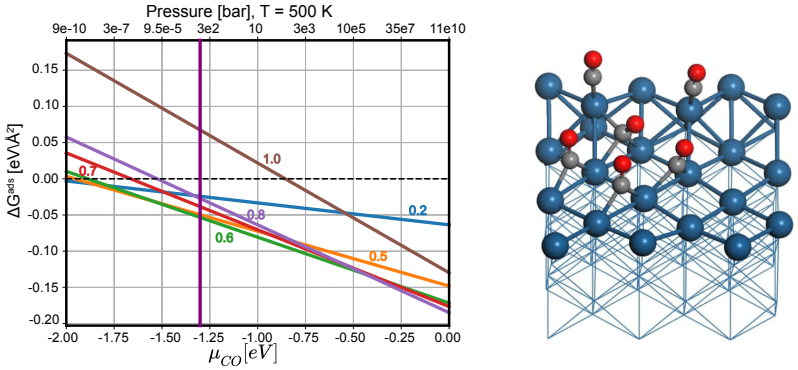

Figure 5.6: Left: Gibbs free energy as a function of CO chemical potential for different CO coverages for Pt(410). Right: Structure with relevant coverage of 0.6 ML chosen for the calculations.

The barrier at the considered experimental conditions is of 2 eV. In figure 5.7, the structures along the reaction coordinated are shown.

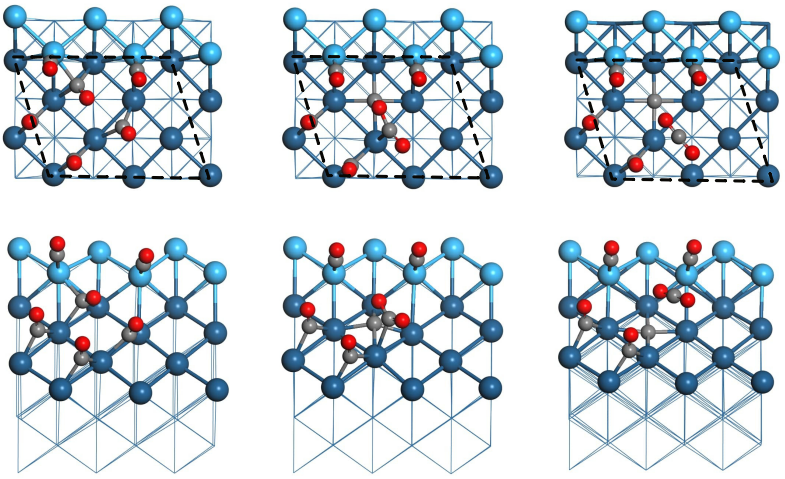

Figure 5.7: Initial, transition and final state for CO dissociation on Pt(410) with a 0.6 ML CO coverage. Top and side. Light blue atoms: Pt atoms of the step. CO coverage = 0.6 ML.

In figure 5.8, the barriers for the reaction on the two chosen model systems are shown.

In conclusion, our results show that CO dissociation can occur on platinum over low-coordinated sites through a Boudouard-like mechanism where two CO molecules react to form CO_2 and leaving carbon adsorbed on the surface. In order for the reaction to occur, high CO coverages are needed in order to destabilize its adsorption. The carbon residues on the surface could then, with

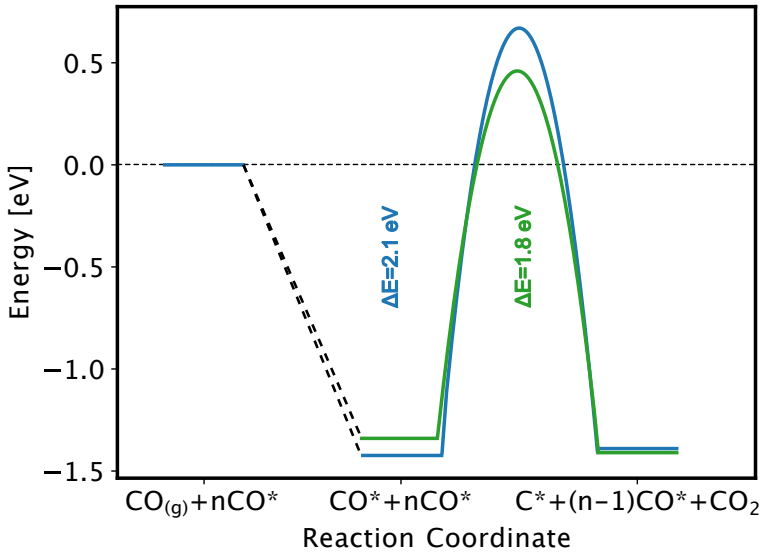

Figure 5.8: Activation energy barrier for CO dissociation over a Pt carbonyl and Pt(410).

the reintroduction of O_2 reoxidize carbon to CO_2. Due to the high CO coverage in the low temperature regime, and to the natural roughness of nanoparticles used in catalysts, CO dissociation might provide a competing reaction to CO oxidation.

5.2 Ceria as an oxide support

Ceria is a reducible oxide that can exist in three forms: stochiometric, partially reduced and reduced. In the pristine case, the valence structure of ceria is composed of a full oxygen 2p band and empty 4f and 5d bands. In the partially reduced case, when an oxygen ion leaves the lattice, the two electrons left behind in the process, localize on two cerium atoms occupying the empty 4f band. In the reduced case, all cerium atoms are in Ce^{3+} state, and the 4f and 5d bands are merged together. A schematic of the electronic structure of ceria for the three cases is shown in figure 5.9.

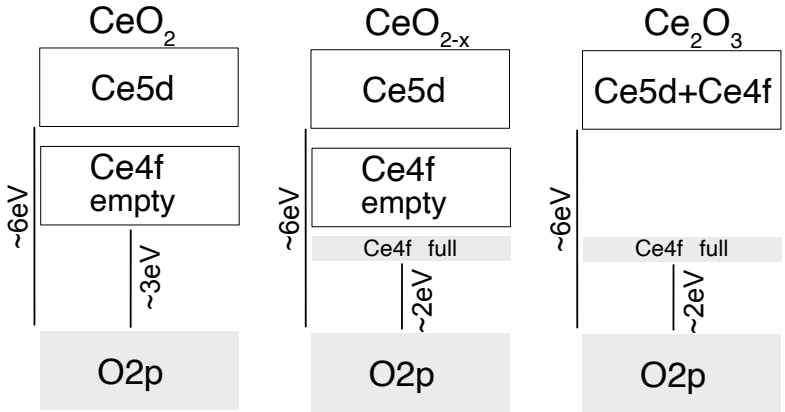

Figure 5.9: Schematic of the electronic structure of ceria for the stochiometric, partially reduced and reduced case respectively, adapted from [110].

The reducibility of ceria is of importance because of the possibility to use oxygen from the lattice as an oxygen buffer, which could reduce the CO poisoning of the catalyst, leading to an improvement of the reaction's activity at low temperature. In this scenario, the reaction path would be the Mars-van Krevelen, which is shown in figure 5.10. In paper III, we carried out a study of CeO_2 and the formation of oxygen vacancies in this oxide.

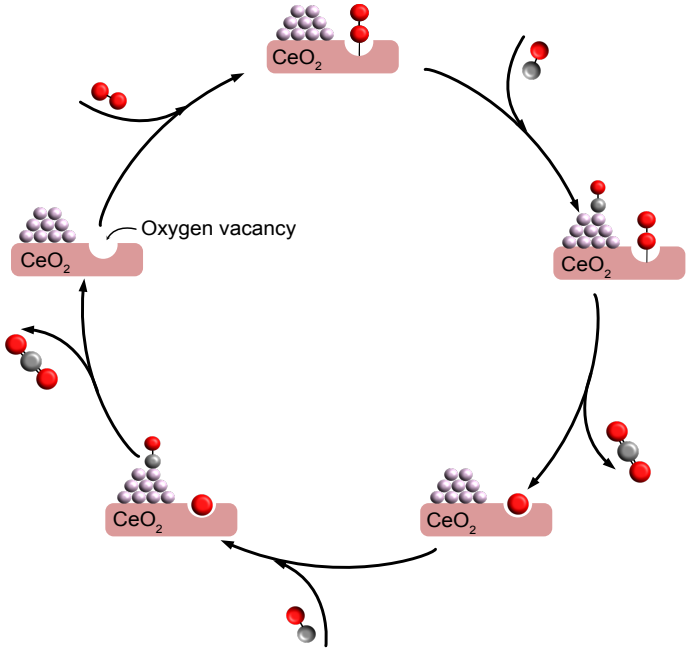

Figure 5.10: Reaction pathway for CO oxidation over ceria supported Pt nanoparticles.

When forming a vacancy in ceria, multiple configurations are possible for the localization of the electrons left behind. In order to avoid delocalization of the f-electrons, we used the PBE+U exchange-correlation functional, which moves the system towards a structure where the occupancy of the f-electrons is complete. Due to the presence of two electrons that need to be localized when a vacancy is formed, the system could be in either a singlet or triplet state. For ceria, the singlet and triplet states are degenerate. We found that when relaxing the system the most frequently found configuration was a nearest neighbors (NN) one. However, a next nearest neighbors (NNN) configuration is preferred by 0.2 eV [111]. The change in oxidation state from Ce^{4+} to Ce^{3+} when an oxygen vacancy is formed, results in elongated O-Ce^{3+} bond lengths. Preparing the structure before relaxation, elongating the bonds of the oxygen atoms with two cerium atoms in NNN position, we managed to find a NNN configuration for the localized electrons. In figure 5.11, the two structures are shown together with the charge density of the cerium atoms where the charge localises.

Due to the structure of ceria, formed by tri-layers of O-Ce-O, we also investigated the formation on the sub-surface. Also in this case, a configuration where the electrons localize on NNN cerium

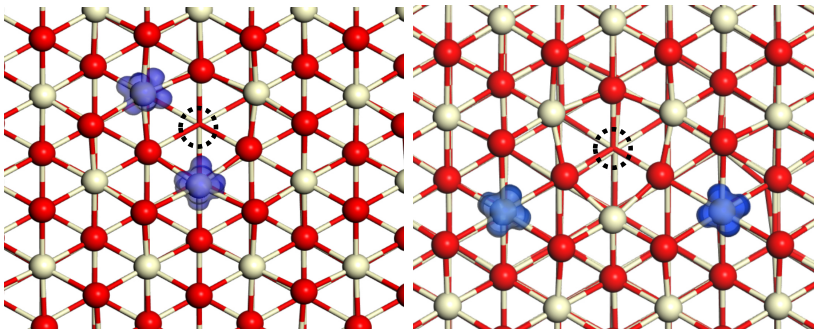

Figure 5.11: Structure and charge density for an oxygen vacancy in CeO_2(111). Left: NN configuration. Right: NNN configuration

atoms is preferred. In such a configuration, the sub-surface vacancy is found to be 0.24 eV more stable than the surface vacancy. The electron localisation strongly depends on the structure relaxation. It has been shown, in fact, that not relaxing the system leads to the electrons delocalisation on three or four cerium atoms [112]. The relaxation breaks the symmetry of the delocalized solution. The subsurface vacancy seems to be preferred since the distortions that arise from the relaxation are longer than in the case of a surface vacancy. The Madelung potential is used to determine the electrostatic potential of an ion in a solid. The ions are, in this case, approximated as single point charges. In metal oxides, the Madelung potential decreases (less attractive) decreasing the vacancy formation energy [113]. In ceria, the NNN position seems to be preferred due to a lower Madelung potential with respect to the NN case [110, 112].

The presence of oxygen vacancies can be experimentally measured with techniques such as STEM. In order to see if other techniques, like XPS, could be used to measure the presence of vacancies, we performed a CLS calculation for the pristine surface and for the vacancy system. In the experimental literature, when XPS measurements are done on ceria systems, usually shifts in the O1s state are assigned to the formation of oxygen vacancies [114–117]. In paper III, we performed core level shifts calculations, in order to understand if the formation of vacancies results in O 1s shifts. From our calculations, we find a CLS of -0.49 eV for the pristine surface and -0.48 eV for the vacancy system. The negative shift of the oxygen vacancy indicates that it is favorable to have the core-hole at the surface with respect to the bulk. Another CLS calculation has been performed when an OH group is present on the surface. For such system, a shift of 2.25 eV is calculated. In figure 5.12, the structures used for the calculations are shown, and in figure 5.13, the CLS calculations are summarized.

Experimentally it is common to assign shifts in the XPS spectra of $\simeq$ 1 eV to the formation of oxygen vacancies [114, 115, 118], however, from our calculations we find that the shifts for the pristine surface and for the vacancy system are very similar. Such similar shifts

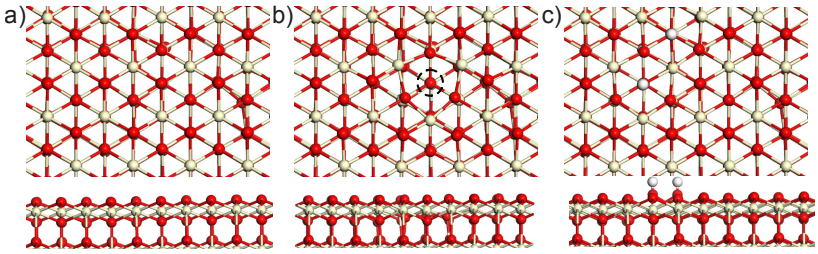

Figure 5.12: a) Pristine CeO_2. b) NNN vacancy on CeO_2. c) Dissociated hydrogen on CeO_2.

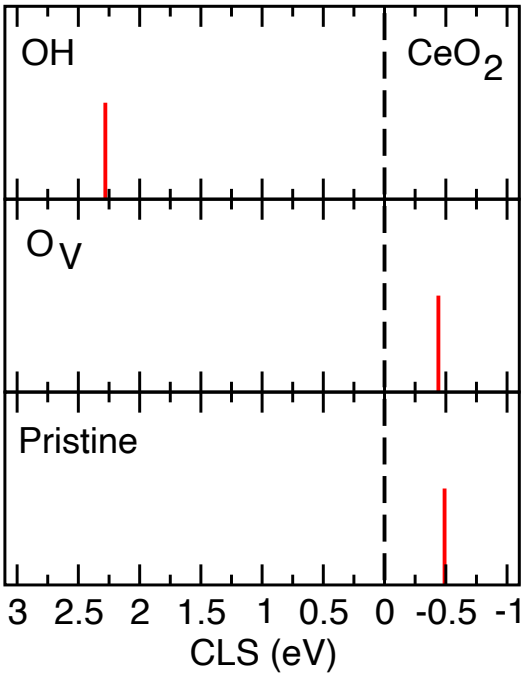

Figure 5.13: CLS calculation. From the top: CLS for adsorbed hydrogen, forming an OH group, vacancy system and pristine surface.

could not be measurable in an XPS experiment, and we suggest that the measured experimental shift could be instead explained by the adsorption of hydrogen on the surface and subsequent formation of OH groups.

5.3 CO oxidation on Pt/CeO_2

In figure 5.10, we show the schematic for the path for CO oxidation over ceria. At low temperatures, when the Pt nanoparticle would be CO poisoned, the CO on the nanoparticle can react with lattice oxygen, resulting in CO_2 and an oxygen vacancy. In the next step, O_2 can then be adsorbed, replenishing the vacancy. CO can then react with one of the O_2 atoms coming back to the original state. To study this reaction and calculate the energies involved, we chose a model system composed of a Pt rod composed by 32 atoms supported on CeO_2(111). This system has been chosen to model a nanoparticle. We decided to keep the ceria lattice constant unchanged, straining the Pt instead. The resulting structure can be seen in figure 5.14.

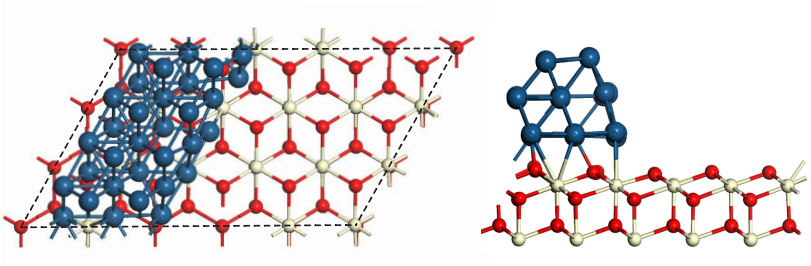

Figure 5.14: Pt rod supported on $CeO_2(111)$. Left: top view. Right: side view.

When single atoms of platinum are adsorbed on a pristine ceria surface, it has been shown that the oxidation state will be +2. When single atoms start to cluster, upon charge redistribution from the ceria to the cluster, the platinum will be in its usual +4 state [119]. From the Bader charge analysis of the system, we see that when the platinum rod is introduced, some charge is transferred from the ceria surface to the rod. This surplus charge will mostly go to the platinum atoms at the interface. Following the previous study on ceria, we know that there will be two free electrons upon the formation of an oxygen vacancy. In order to understand if these electrons would delocalise on Pt or localise on ceria, we performed density of state calculations for the vacancy system, presented in figure 5.15. In this system, the vacancy formation energy results to

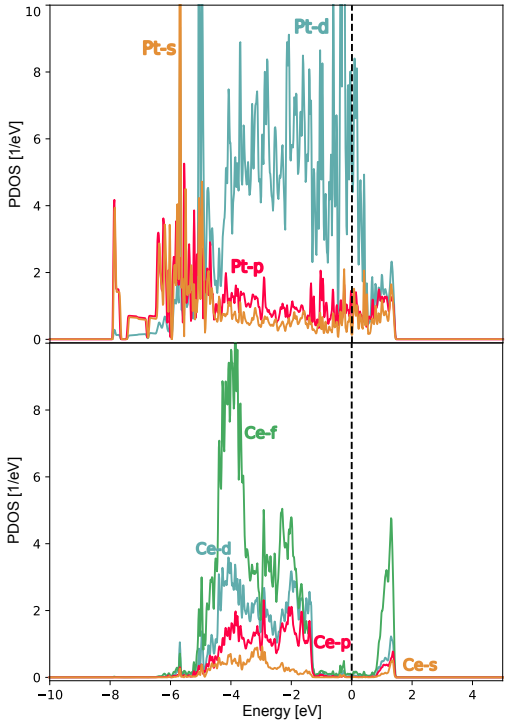

Figure 5.15: Top: Projected DOS for Pt. Bottom: Projected DOS for ceria.

be 1.92 eV, which is 0.24 eV less endothermic than on $CeO_2(111)$. In table 5.1 adsorption energies for CO and O on different sites of the rod are shown.

With respect to the previous studies on CO and O adsorption on

E_{ads} (eV)	CO	O
a-top	-1.97	-0.84
bridge	-1.98	-1.61
Top of the rod	-1.71	-1.81

Table 5.1: Adsorption energies of CO and O on different sites of the supported Pt rod.

platinum, we find that CO adsorbs less strongly on the Pt/CeO_2 system than on Pt(100) and Pt(211), while it adsorbs more strongly than on Pt(111). At the same time, oxygen has a stronger adsorption energy in the bridge site on the rod system than on Pt(111), Pt(100) and Pt(211). The localization of the charge on cerium atoms seems to be of vital importance for the reaction on the system, see figure 5.14. In figure 5.16, we show the potential energy landscape for the reaction when the charge coming from the formation of the vacancy does not localize on ceria and when it does localize on ceria forming two Ce^{3+} atoms, respectively. As can be seen, the

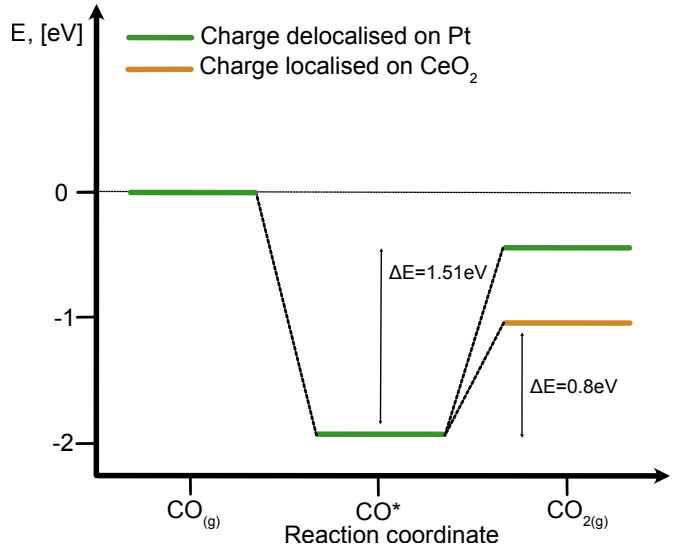

Figure 5.16: Potential energy landscape for CO oxidation over a ceria supported Pt rod. Green line: the charge from the formation of the vacancy does not localize on cerium atoms. Orange line: the charge from the formation of the vacancy localizes on cerium atoms forming two Ce^{3+} atoms.

reaction is endothermic, but the charge localization reduces the ΔE between the two basin states. At the regime of interest, which is at low temperature, the CO coverage on platinum is high, causing CO poisoning, so we decided to consider a higher CO coverage in our calculations. Multiple calculations have been performed, in order to find the most stable configuration with a 0.7 ML CO coverage. The resulting structure is shown in figure 5.17.

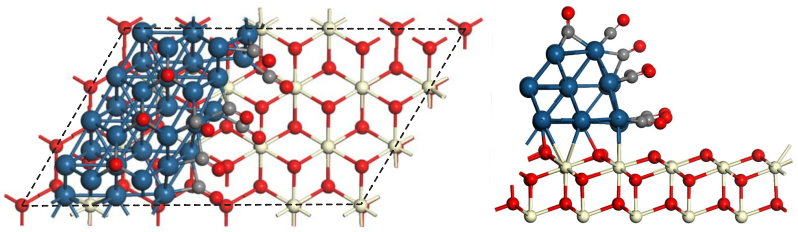

Figure 5.17: Pt rod supported on CeO_2(111) at 0.7 ML CO coverage. Left: top view. Right: side view.

For the most stable configuration the adsorption energy of CO is

reduced to -1.24 eV. As can be seen in figure 5.18, when the coverage is high, the reaction is exothermic by 0.3 eV; both the potential energy landscape and the Gibbs free energy are shown. The Gibbs free energy has been calculated at 300 K.

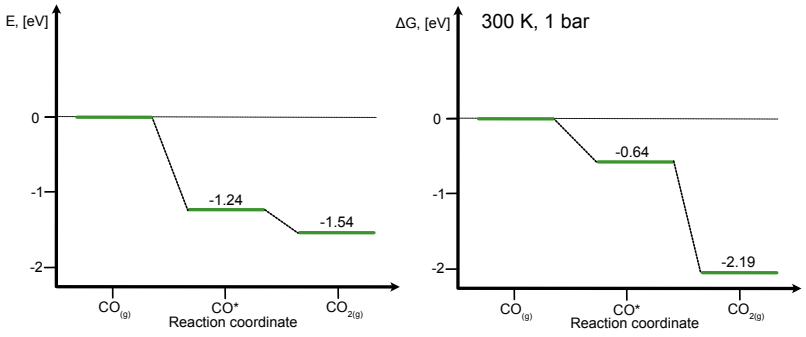

Figure 5.18: Left: Potential energy landscape for CO oxidation over ceria supported Pt rod for a CO coverage of 0.7 ML. Right: Gibbs free energy for CO oxidation over ceria supported Pt rod for a CO coverage of 0.7 ML at 300 K.

Under these assumptions, we started performing NEB calculations to find the activation energy of the reaction between a CO molecule on an interface site of the rod and a lattice oxygen in ceria. These calculation results to be complex on such a system, where upon the formation of an oxygen vacancy, the charge need to localize on the cerium atoms. The electrons can, in fact, move back and forth between the cerium atoms and the platinum rod, creating complex lattice oscillations, which make the calculations difficult to converge.

Conclusions and future work 6

The main objective of this thesis has been to get an understanding of CO oxidation in the low temperature regime. This has been obtained by studying a model system that experimentally has shown high activity at low temperature, namely Pt/CeO_2. A bottom up approach has been applied, investigating both the separated components (Pt and CeO_2) and the combined system. The methodology that has been used is density functional theory (DFT) combined with kinetic Monte Carlo (kMC) simulations.

Many steps towards the main goal have been achieved, providing some general understanding. Starting from platinum, we studied CO dissociation as a possible competing reaction to CO oxidation at low temperatures. Combining DFT calculations with experimental work, it is shown that at low temperature regimes, some structures might give rise to special sites where CO dissociation becomes possible. CO dissociation might, in this case, represent a competing reaction to CO oxidation. The dissociation proceeds through a Boudouard pathway, where two CO molecules react, forming CO_2 and leaving carbon residues on the surface. These residues poison the surface, and the structures which showed such poisoning, also presented a higher light-off temperature for the subsequent CO oxidation reaction. Experimentally, there is clear evidence of CO dissociation, and subsequent carbon poisoning on platinum. However, the activation barriers found for the studied model systems (Pt(410) and Pt carbonyl), are about 2 eV. These values are lower than for the barriers found on Pt(111) and Pt(100) for direct dissociation, but they are still high. This suggests that the chosen model systems might not reflect the experimental situation, and that further investigation could be necessary. Such work could provide interesting insights on the modeling of real catalysts, in order to avoid structures where CO dissociation can occur.

This work also contains the investigation on a widely used tool, namely linear scaling relations. Linear scaling relations relate the adsorption energy of reactants with a descriptor such as generalized coordination number or d-band center and provide a way to describe the complete potential energy surface for systems where different adsorption sites are present, without the need for expensive computational time. It is shown that the kinetics of the system does not show a strong dependency on the slope of such relations. Furthermore, it has been shown how the kinetics does not seem to be dependent on structural dependent parameters such as the oxygen sticking coefficient. This justifies the use of approximations

to these values. This study corroborates the use of scaling relation for kinetics study. However, such relations depend on the reactants and on the metal used as a catalyst. This means that our results can not be generalized, and similar studies should be carried out for other metal catalysts. Furthermore, linear scaling relations are rare for oxides. For oxide catalysts or metal/oxide systems, a complete screening of the potential energy landscape would be necessary.

We moved then to the investigation of ceria as an oxide support. The formation of surface oxygen vacancies has been investigated, showing that different structures are possible. It has been shown through core level shifts (CLS) calculations that these vacancies should not be visible in O1s XPS measurements. This result that the experimental assignment of such shift to oxygen defects probably should be reconsidered.

The knowledge obtained for the separated systems was used to study CO oxidation over ceria supported platinum nanoparticles. The presence of two electrons that need to be localised upon the formation of an oxygen vacancy and the possibility for them to localise in different configurations, make ceria a complicated system to study computationally. The localisation of the electrons, plays a role in the vacancy formation energy. The difference in vacancy formation energy is reflected in the potential energy landscape. It is shown that depending on the electronic localisation, the reaction can be more or less endothermic. This means that it is important to monitor where the electrons go, assuring their localisation on ceria and not a delocalisation on platinum. For this system, we also investigated the kinetics. Our results show an activity at low temperature higher than on Pt(111) and than on platinum nanoparticles. It is interesting to notice that this activity is not due to lower activation barriers for CO oxidation. The higher activity, in fact, derives from the possibility at low temperatures for the reaction to follow a Mars-van Krevelen mechanism. This suggests that the kinetics could be further improved, but modifying the investigated system. The activation barrier for the reaction, depends on the vacancy formation energy. Doping the system could, for example, lower the vacancy formation energy and, in this way, lower the activation barrier, further increasing the turnover frequency at low temperatures.

In conclusion, the present work shows that the low temperature regime leads to many challenges. On one hand the reaction is inactive at low temperatures on platinum, due to the strong binding energy of CO. In addition, reactions like CO dissociation might become possible when performing the reaction on rough nanoparticles, which further hinders low temperature CO oxidation. Despite the controversial topic of CO dissociation on platinum, theoretical and

experimental work seem to prove this as a possibility on rough Pt-systems. These results have contributed to a better understanding of the difficulties encountered in the low temperature regime, underlying once more the important role of the catalyst's morphology. This understanding could provide inspiration for the fabrication of catalysts. Moreover, it has been made clear how a different pathway might make a reaction possible. This is of particular interest when studying the CO oxidation on ceria. In this case, the reaction at low temperature proceeds through a Mars-van Krevelen mechanism, while at higher temperatures, it will proceed on platinum through the Langmuir-Hinshelwood mechanism. Such result implies that a reaction might become possible even though the activation barriers are similar to the ones we would have on pristine platinum, by simply providing another route.

6.1 Outlook

The goal of this project is to provide an understanding of CO oxidation at low temperatures, which lead us to study systems such as CeO_2. Several questions still need to be answered. In our work CO oxidation seems to have a high activity at low temperatures, due to the possibility to use lattice oxygen instead of oxygen adsorbed on Pt. This enables a low temperature activity. The activation energies that we have obtained for the Mars-van Krevelen mechanism are not lower than the barriers for CO oxidation on platinum through the Langmuir-Hinshelwood mechanism. Thus, the low temperature activity is a consequence of not being sensitive to CO poisoning. There is room for further improvement by lowering the barriers for O-CO coupling. One route might be doping the oxide with the same metal atoms the nanoparticles are composed of, in this case, platinum. The doping could lower the energy needed to form an oxygen vacancy, and at the same time destabilize the adsorption of CO, resulting in a lower activation barrier. Furthermore, it could be interesting to modify the structure of the ceria support, studying, for example, nanosized ceria. Nanosized ceria has shown, in fact, the possibility of oxygen spillover. In addition, the vacancy formation energy seems to depend on the size of the nanoparticles. Both these effects could lead to lower activation barriers and different pathways for the reaction.

Acknowledgements

The research presented herein was carried out at the Division of Chemical Physics and Competence Centre for Catalysis at Chalmers University of Technology, Göteborg, Sweden in the period November 2018 to April 2021.

The research was funded by Competence Centre for Catalysis at Chalmers University of Technology.

The Competence Centre for Catalysis is financially supported by Chalmers University of Technology, the Swedish Energy Agency, and the member companies: AB Volvo, ECAPS AB, Johnson Matthey AB, Preem AB, Scania CV AB and Umicore Denmark ApS.

Computational time was granted by SNIC at C3SE (Göteborg), PDC (Stockholm) and Uppmax (Uppsala).

Additionally, I would like to thank:

My main supervisor, Henrik Grönbeck. Thank you for being so supportive and always finding the time to discuss science and personal development.

My co-supervisor and collaborators, Anders Hellman, Magnus Skoglundh, Per-Anders Carlsson and Jojo for the fruitful discussions and comments.

All my colleagues at Chemical Physics are acknowledged. Thanks for creating a chill and pleasant working environment.

I'd like to especially thank: Alva(b)ro, who replied to an infinite amount of questions (almost) never complaining, and who told me that I should acknowledge him "...not only as a coworker, but as a friend. If you're going to quote that, then you should also add mentor" which I tend to agree with most days, and Rosemary, who became in such a short time one of the best friends I've ever had, and that I miss dearly, I love you loads.

I also can not forget the friends from Italy. Erika, my university companion with whom I could sing ABBA to kill the pre-exam anxiety and without whom I probably wouldn't be here, ti voglio bene. My brothers, di sangue e non, che porto sempre con me and Andre (very sus) that supported me for the last 11 years (ck).

And of course my dad and my mom, il cui altruismo e forza sono da invidiare. Grazie per sostenermi nonostante i miei molteplici dubbi sulla vita, ti voglio bene.

Noemi Bosio, Göteborg, March 2021

Bibliography

[1] J. Hansen, M. Sato, R. Ruedy, K. Lo, D. W Lea and M. Medina-Elizade. 'Global temperature change'. In: *Proceedings of the National Academy of Sciences* 103.39 (2006), pp. 14288–14293. DOI: 10.1073/pnas.0606291103 (cit. on p. 1).

[2] S. A. Zimov, E. A. G. Schuur and F. S. Chapin. 'Permafrost and the Global Carbon Budget'. In: *Science* 312.5780 (2006), pp. 1612–1613. DOI: 10.1126/science.1128908 (cit. on p. 1).

[3] G. A. Meehl and C. Tebaldi. 'More Intense, More Frequent, and Longer Lasting Heat Waves in the 21st Century'. In: *Science* 305.5686 (2004), pp. 994–997. DOI: 10.1126/science.1098704 (cit. on p. 1).

[4] M. P. B. Musculus, P. C. Miles and L. M. Pickett. 'Conceptual models for partially premixed low-temperature diesel combustion'. In: *Progress in Energy and Combustion Science* 39.2 (2013), pp. 246–283. DOI: https://doi.org/10.1016/j.pecs.2012.09.001 (cit. on p. 1).

[5] I. Lefort, J. M. Herreros and A. Tsolakis. 'Reduction of Low Temperature Engine Pollutants by Understanding the Exhaust Species Interactions in a Diesel Oxidation Catalyst'. In: *Environmental Science & Technology* 48.4 (Feb. 2014), pp. 2361–2367. DOI: 10.1021/es4051499 (cit. on p. 1).

[6] I. Chorkendorff and J. W. Niemantsverdriet. *Concepts of Modern Catalysis and Kinetics*. English. Newark, 2017. URL: https://search.ebscohost.com/login.aspx?direct=true&scope=site&db=nlebk&db=nlabk&AN=1535819 (cit. on pp. 1, 30, 31).

[7] S. Semlitsch, S. Torron, M. Johansson and M. Martinelle. 'Enzymatic catalysis as a versatile tool for the synthesis of multifunctional, bio-based oligoester resins'. In: *Green Chemistry* 18.7 (2016), pp. 1923–1929. DOI: 10.1039/C5GC02597D (cit. on p. 1).

[8] A. Renken M. Beller and Rutger A. van Santen. 'Catalysis. From Principles to Applications.' In: *Angewandte Chemie - International Edition* 52.10 (2013), p. 2650. DOI: https://doi.org/10.1002/anie.201210089 (cit. on pp. 1, 4).

[9] E. W. Kuipers, A. Vardi, A. Danon and A. Amirav. 'Surface-molecule proton transfer: A demonstration of the Eley-Rideal mechanism'. In: *Physical Review Letters* 66 (1 Jan. 1991), pp. 116–119. DOI: 10.1103/PhysRevLett.66.116 (cit. on p. 2).

[10] J. R. H. Ross. 'Chapter 7 - The Kinetics and Mechanisms of Catalytic Reactions'. In: *Contemporary Catalysis*. Ed. by Julian R H Ross. Amsterdam: Elsevier, 2019, pp. 161–186. DOI: https://doi.org/10.1016/B978-0-444-63474-0.00007-2 (cit. on p. 2).

[11] H. J. Freund, G. Meijer, M. Scheffler, R. Schlögl and W. Martin. 'CO oxidation as a prototypical reaction for heterogeneous processes'. In: *Angewandte Chemie* 50 (2011), pp. 10064–10094 (cit. on p. 2).

[12] T. Engel and G. Ertl. 'A molecular beam investigation of the catalytic oxidation of CO on Pd(111)'. In: *Journal of Chemical Physics* 69 (1978), p. 1267. DOI: https://doi.org/10.1063/1.436666 (cit. on p. 2).

[13] C. T. Campbell, G. Ertl, H. Kuipers and J. Segner. 'A molecular beam investigation of the interactions of CO on a Pt(111) surface'. In: *Journal of Chemical Physics* 107.11 (1981), pp. 207–219 (cit. on p. 2).

[14] R. Imbihl and G. Ertl. 'Oscillatory kinetics in heterogeneous catalysis'. In: *Chemical Reviews* 95.3 (1995), pp. 697–733. DOI: 10.1021/cr00035a012 (cit. on p. 3).

[15] M. Eiswirth, J. Bürger, P. Strasser and G. Ertl. 'Oscillating LangmuirHinshelwood Mechanisms'. In: *The Journal of Physical Chemistry* 100.49 (Jan. 1996), pp. 19118–19123. DOI: 10.1021/jp961688y (cit. on p. 3).

[16] B. C. Sales, J. E. Turner and M. B. Maple. 'Oscillatory oxidation of CO over Pt, Pd and Ir catalysts: Theory'. In: *Surface Science* 114.2 (1982), pp. 381–394. DOI: https://doi.org/10.1016/0039-6028(82)90692-6 (cit. on p. 3).

[17] J. E. Turner and M. B. Maple. 'Oxide formation and reduction over Pt, Pd, and Ir; A driving mechanism for oscillations in the co oxidation reaction'. In: *Surface Science* 147.2 (1984), pp. 647–662. DOI: https://doi.org/10.1016/0039-6028(84)90476-X (cit. on p. 3).

[18] R. J. Gelten, A. P. J. Jansen, R. A. van Santen, J. J. Lukkien, J. P. L. Segers and P. A. J. Hilbers. 'Monte Carlo simulations of a surface reaction model showing spatio-temporal pattern formations and oscillations'. In: *The Journal of Chemical Physics* 108.14 (1998), pp. 5921–5934. DOI: 10.1063/1.476003 (cit. on p. 3).

[19] A. J. Medford, A. Vojvodic, J. S. Hummelshøj, J. Voss, F. Abild-Pedersen, F. Studt, T. Bligaard, A. Nilsson and J. K. Nørskov. 'From the Sabatier principle to a predictive theory of transition-metal heterogeneous catalysis'. In: *Journal of Catalysis* 328 (2015), pp. 36–42. DOI: https://doi.org/10.1016/j.jcat.2014.12.033 (cit. on p. 4).

[20] J. T. Kummer. 'Use of noble metals in automobile exhaust catalysts'. In: *Journal of Physical Chemistry* 90.20 (1986), pp. 4747–4752. DOI: 10.1021/j100411a008 (cit. on p. 4).

[21] S. H. Taylor, G. J. Hutchings and A. A. Mirzaei. 'Copper zinc oxide catalysts for ambient temperature carbon monoxide oxidation'. In: *Chemical Communications* 15 (1999), pp. 1373–1374. DOI: 10.1039/a903426i (cit. on p. 4).

[22] L. H. Chang, N. Sasirekha, B. Rajesh and Y. W. Chen. 'CO oxidation on ceria- and manganese oxide-supported gold catalysts'. In: *Separation and Purification Technology* 58.1 (2007), pp. 211–218. DOI: 10.1016/j.seppur.2007.07.031 (cit. on p. 4).

[23] K. An, S. Alayoglu, N. Musselwhite, S. Plamthottam, G. Melaet, A. E. Lindeman and G. A. Somorjai. 'Enhanced CO Oxidation Rates at the Interface of Mesoporous Oxides and Pt Nanoparticles'. In: *Journal of the American Chemical Society* 135.44 (Nov. 2013), pp. 16689–16696. DOI: 10.1021/ja4088743 (cit. on p. 4).

[24] R. Mandapaka and G. Madras. 'Aluminium and rhodium co-doped ceria for water gas shift reaction and CO oxidation'. In: *Molecular Catalysis* 451 (2018), pp. 4–12. DOI: 10.1016/j.mcat.2017.10.001 (cit. on p. 4).

[25] F. Maurer, J. Jelic, J. Wang, A. Gänzler, P. Dolcet, C. Wöll, Y. Wang, F. Studt, M. Casapu and J. D. Grunwaldt. 'Tracking the formation, fate and consequence for catalytic activity of Pt single sites on CeO2'. In: *Nature Catalysis* 3.10 (2020), pp. 824–833. DOI: 10.1038/s41929-020-00508-7 (cit. on p. 5).

[26] G. N. Vayssilov, Y. Lykhach, A. Migani, T. Staudt, G. P. Petrova, N. Tsud, T. Skála, A. Bruix, F. Illas, K. C. Prince, V. Matolín, K. M. Neyman and J. Libuda. 'Support nanostructure boosts oxygen transfer to catalytically active platinum nanoparticles'. In: *Nature Materials* 10.4 (2011), pp. 310–315. DOI: 10.1038/nmat2976 (cit. on p. 5).

[27] H. Y. Kim and G. Henkelman. 'CO oxidation at the interface between doped CeO 2 and supported Au nanoclusters'. In: *Journal of Physical Chemistry Letters* 3.16 (2012), pp. 2194–2199. DOI: 10.1021/jz300631f (cit. on p. 5).

[28] L. Li, A. H. Larsen, N. A. Romero, V. A. Morozov, C. Glinsvad, F. Abild-Pedersen, J. Greeley, K. W. Jacobsen and J. K. Nørskov. 'Investigation of catalytic finite-size-effects of platinum metal clusters'. In: *Journal of Physical Chemistry Letters* 4.1 (2013), pp. 222–226. DOI: 10.1021/jz3018286 (cit. on p. 5).

[29] J. Kleis, J. Greeley, N. A. Romero, V. A. Morozov, H. Falsig, A. H. Larsen, J. Lu, J. J. Mortensen, M. Dułak, K. S. Thygesen, J. K. Nørskov and K. W. Jacobsen. 'Finite size effects in chemical bonding: From small clusters to solids'. In: *Catalysis Letters* 141.8 (2011), pp. 1067–1071. DOI: 10.1007/s10562-011-0632-0 (cit. on p. 5).

[30] I. V. Yudanov, R. Sahnoun, K. M. Neyman, N. Rösch, J. Hoffmann, S. Schauermann, V. Johánek, H. Unterhalt, G. Rupprechter, J. Libuda and H. J. Freund. 'CO adsorption on Pd nanoparticles: Density functional and vibrational spectroscopy studies'. In: *JOurnal of Physical Chemistry B* 107.1 (2003), pp. 255–264. DOI: 10.1021/jp022052b (cit. on p. 5).

[31] S. Syrenova, C. Wadell, F. A. A. Nugroho, T. A. Gschneidtner, Y. A. Diaz Fernandez, G. Nalin, D. Switlik, F. Westerlund, T. J. Antosiewicz, V. P. Zhdanov, K. Moth-Poulsen and C. Langhammer. 'Hydride formation thermodynamics and hysteresis in individual Pd nanocrystals with different size and shape'. In: *Nature Materials* 14.12 (2015), pp. 1236–1244. DOI: 10.1038/nmat4409 (cit. on p. 5).

[32] J. Libuda, I. Meusel, J. Hoffmann, J. Hartmann, L. Piccolo, C. R. Henry and H. J. Freund. 'The CO oxidation kinetics on supported Pd model catalysts: A molecular beam/in situ time-resolved infrared reflection absorption spectroscopy study'. In: *Journal of Chemical Physics* 114.10 (2001), pp. 4669–4684. DOI: 10.1063/1.1342240 (cit. on p. 5).

[33] C. Papp. 'From flat surfaces to nanoparticles: In situ studies of the reactivity of model catalysts'. In: *Catalysis Letters* 147.1 (2017), pp. 2–19. DOI: 10.1007/s10562-016-1925-0 (cit. on p. 5).

[34] K. Reuter. 'Insight into a pressure and materials gap: CO oxidation at "ruthenium" catalysts'. In: *Oil and Gas Science and Technology* 61.4 (2006), pp. 471–477. DOI: 10.2516/ogst:2006027a (cit. on p. 5).

[35] P. A. M. Dirac. 'Quantum Mechanics of Many-Electron Systems.' In: *Proceedings of the royal society B* 123.792 (1929), pp. 714–733 (cit. on p. 7).

[36] A. Szabo and N. S. Ostlund. *Modern Quantum Chemistry: Introduction to Advanced electronic structure theory*. Mineola, New York: Dover Publications, 1996 (cit. on p. 7).

[37] J. Kohanoff. *Electronic Structure Calculations for Solids and Molecules: Theory and Computational Methods*. New York (USA): Cambridge University Press, 2006 (cit. on p. 8).

[38] D. R. Hartree. 'The wave mechanics of an atom with a non-Coulomb central field Part I Theory and methods'. In: *Mathematical Proceedings of the Cambridge Philosophical Society* 24.1 (1928), pp. 89–110 (cit. on p. 8).

[39] V. Fock. 'Näherungsmethode zur Lösung des quantenmechanischen Mehrkörperproblems'. In: *Zeitschrift für Physik* 61.1 (1930), pp. 126–148. DOI: 10.1007/BF01340294 (cit. on p. 8).

[40] J. C. Slater. 'The theory of complex spectra'. In: *Physical Review* 34.10 (1929), pp. 1293–1322. DOI: 10.1103/PhysRev.34.1293 (cit. on p. 8).

[41] L. H. Thomas. 'The calculation of atomic fields'. In: *Mathematical Proceedings of the Cambridge Philosophical Society* 23.5 (1927), pp. 542–548. DOI: 10.1017/S0305004100011683 (cit. on p. 8).

[42] E. Fermi. 'Un metodo statistico per la determinazione di alcune prioritá dell'atomo'. In: *Accademia nazionale dei Lincei* 6 (1927), pp. 602–6070 (cit. on p. 8).

[43] P. Hohenberg and W. Kohn. 'Inhomogeneous electron gas'. In: *Physical Review* 136.3B (1964), B864–B871. DOI: 10.1133/PhysRev.136.B864 (cit. on pp. 9, 11).

[44] W. Kohn and L. J. Sham. 'Self-consistent equations including exchange and correlation effects'. In: *Physical Review* 140.4A (1965), A1133–A1138. DOI: 10.1133/PhysRev.140.A1133 (cit. on p. 9).

[45] A. F. Janak. 'Proof that $\frac{\delta E}{\delta n_i} = \epsilon_i$ in density-functional theory'. In: *Physical Review B* 18.12 (1978), pp. 7165–7168. DOI: 10.1103/PhysRevB.18.7165 (cit. on p. 11).

[46] J. P. Perdew, A. Ruzsinszky, J. Tao, V. N. Staroverov, G. E. Scuseria and G. I. Csonka. 'Prescription for the design and selection of density functional approximations: More constraint satisfaction with fewer fits'. In: *Journal of Chemical Physics* 123.6 (2005). DOI: 10.1063/1.1904565 (cit. on pp. 11, 12).

[47] Jones, R. O. and Gunnarsson, O. 'The density functional formalism, its applications and prospects'. In: *Reviews of Modern Physics* 77 (1989), pp. 689–818. DOI: 10.1103/RevModPhys.61.689 (cit. on p. 12).

[48] J. P. Perdew, K. Burke and M. Ernzerhof. 'Generalized gradient approximation made simple'. In: *Physical Review Letters* 77.18 (1996), pp. 3865–3868. DOI: 10.1103/PhysRevLett.77.3865 (cit. on p. 12).

[49] V. Polo, E. Kraka and D. Cremer. 'Electron correlation and the self-interaction error of density functional theory'. In: *Molecular Physics* 100.11 (2002), pp. 1771–1790. DOI: 10.1080/00268970110111788 (cit. on p. 12).

[50] R. Neumann and N. C. Handy. 'Higher-order gradient corrections for exchange-correlation functionals'. In: *Chemical Physics Letters* 266.1-2 (1997), pp. 16–22. DOI: 10.1016/S0009-2614(96)01496-0 (cit. on p. 13).

[51] J. P. Perdew and A. Zunger. 'Self-interaction correction to density-functional approximations for many-electron systems'. In: *Physical Review B* 23 (10 May 1981), pp. 5048–5079. DOI: 10.1103/PhysRevB.23.5048 (cit. on p. 13).

[52] S. Lehtola and H. Jónsson. 'Variational, Self-Consistent Implementation of the Perdew–Zunger Self-Interaction Correction with Complex Optimal Orbitals'. In: *Journal of Chemical Theory and Computation* 10.12 (Dec. 2014), pp. 5324–5337. DOI: 10.1021/ct500637x (cit. on p. 13).

[53] A. D. Becke. 'Density-functional thermochemistry. III. The role of exact exchange'. In: *The Journal of Chemical Physics* 98.7 (1993), pp. 5648–5652. DOI: 10.1063/1.464913 (cit. on p. 13).

[54] V. I. Anisimov, J. Zaanen and O. K. Andersen. 'Band theory and Mott insulators: Hubbard U instead of Stoner I'. In: *Physical Review B* 44.3 (1991), pp. 943–954. DOI: 10.1103/PhysRevB.44.943 (cit. on p. 13).

[55] Lundqvist, B. I. and Andersson, J. and Shao, H. and Chan, S. and Langreth, D. C. 'Density functional theory including Van Der Waals forces'. In: *Quantum Chemistry* 56.4 (1995), pp. 247–255. DOI: 10.1002/qua.560560410 (cit. on p. 13).

[56] G. Kresse and J. Furthmuller. 'Efficient iterative schemes for ab initio total-energy calculations using a plane-wave basis set'. In: *Physical Review B* 54.16 (1996), pp. 11169–11186. DOI: 10.1103/PhysRevB.54.11169 (cit. on p. 14).

[57] P. E. Blöchl. 'Projector augmented-wave method'. In: *Physical Review B* 50.24 (1994), pp. 17953–17979. DOI: 10.1103/PhysRevB.50.17953 (cit. on p. 15).

[58] R. P. Feynman. 'Forces in Molecules'. In: *Physical Reviews* 56 (4 Aug. 1939), pp. 340–343. DOI: 10.1103/PhysRev.56.340 (cit. on p. 17).

[59] M. E. H. Ismail and R. Zhang. 'On the Hellmann-Feynman theorem and the variation of zeros of certain special functions'. In: *Advances in Applied Mathematics* 9.4 (1988), pp. 439–446. DOI: https://doi.org/10.1016/0196-8858(88)90022-X (cit. on p. 17).

[60] R. M. Martin. *Electronic Structure: Basic Theory and Practical Methods*. Cambridge University Press, 2004 (cit. on p. 17).

[61] P. D. Nellist. 'The Principles of STEM Imaging'. In: *Scanning Transmission Electron Microscopy: Imaging and Analysis*. Ed. by Stephen J Pennycook and Peter D Nellist. New York, NY: Springer New York, 2011, pp. 91–115. DOI: 10.1007/978-1-4419-7200-2_2 (cit. on p. 17).

[62] J. Evans. 'Introduction to X-Ray Absorption Fine Structure (XAFS)'. In: *X-Ray Absorption Spectroscopy for the Chemical and Materials Sciences*. John Wiley & Sons, Ltd, 2018. Chap. 1, pp. 1–8. DOI: https://doi.org/10.1002/9781118676165.ch1 (cit. on p. 18).

[63] G. Henkelman, B. P. Uberuaga and H. Jónsson. 'Climbing image nudged elastic band method for finding saddle points and minimum energy paths'. In: *Journal of Chemical Physics* 113.22 (2000), pp. 9901–9904. DOI: 10.1063/1.1329672 (cit. on pp. 18, 19).

[64] J. Baker. 'Molecular Structure and Vibrational Spectra'. In: *Handbook of Computational Chemistry*. Ed. by Jerzy Leszczynski. Dordrecht: Springer Netherlands, 2012, pp. 293–359. DOI: 10.1007/978-94-007-0711-5_10 (cit. on p. 20).

[65] G. D. Christian. 'Spectrochemical Methods'. In: *Analytical chemistry*. John Wiley & Sons, Ltd, 2015. Chap. 16, pp. 477–548 (cit. on p. 20).

[66] H. Eyeing. 'The activated complex and the absolute rate of chemical reactions'. In: *Chemical Reviews* 17.1 (1935), pp. 65–77. DOI: 10.1021/cr60056a006 (cit. on pp. 20, 21).

[67] G. Mills, H. Jónsson and G. K. Schenter. 'Reversible work transition state theory: application to dissociative adsorption of hydrogen'. In: *Surface Science* 324.2-3 (1995), pp. 305–337. DOI: 10.1016/0039-6028(94)00731-4 (cit. on pp. 20–22).

[68] K. Reuter and M. Scheffler. 'Composition, structure, and stability of RuO_2(110) as a function of oxygen pressure'. In: *Physical Review B* 65 (3 Dec. 2001), p. 035406. DOI: 10.1103/PhysRevB.65.035406 (cit. on p. 22).

[69] Q. Sun, K. Reuter and M. Scheffler. 'Effect of a humid environment on the surface structure of RuO_2(110)'. In: *Physical Review B* 67 (20 May 2003), p. 205424. DOI: 10.1103/PhysRevB.67.205424 (cit. on p. 22).

[70] K. Reuter, C. Stampf and M. Scheffler. 'AB Initio Atomistic Thermodynamics and Statistical Mechanics of Surface Properties and Functions'. In: *Handbook of Materials Modeling: Methods*. Ed. by Sidney Yip. Dordrecht: Springer Netherlands, 2005, pp. 149–194. DOI: 10.1007/978-1-4020-3286-8_10 (cit. on p. 22).

[71] P. J. Linstrom and W. G. Mallard. *NIST Chemistry WebBook*. 2005. URL: https://webbook.nist.gov (cit. on p. 23).

[72] K. Siegbahn, C. Nordling and A. Fahlman. *ESCA, atomic, molecular and solid state structure studied by means of electron spectroscopy*. Tech. rep. Uppsala: Almqvist and Wiksell, 1967 (cit. on p. 24).

[73] F. Hofmann. *Auger- and X-Ray Photoelectron Spectroscopy in Materials Science*. Berlin, Heidelberg: Springer-Verlag: Springer Series in Surface Sciences, 2013 (cit. on p. 24).

[74] J. N. Andersen, D. Hennig, E. Lundgren, M. Methfessel, R. Nyholm and M. Scheffler. 'Surface core-level shifts of some 4d-metal single-crystal surfaces: Experiments and ab initio calculations'. In: *Physical Review B* 50.23 (1994), pp. 17525–17533. DOI: 10.1103/PhysRevB.50.17525 (cit. on p. 24).

[75] E. Pehlke and M. Scheffler. 'Evidence for site-sensitive screening of core holes at the Si and Ge (001) surface'. In: *Physical Review Letters* 71.14 (1993), pp. 2338–2341. DOI: 10.1103/PhysRevLett.71.2338 (cit. on p. 25).

[76] A. Posada-Borbón, N. Bosio and H. Grönbeck. 'On the signatures of oxygen vacancies in O1s core level shifts'. In: *Surface Science* 705.October 2020 (2021), pp. 1–5. DOI: 10.1016/j.susc.2020.121761 (cit. on p. 25).

[77] L. Köhler and G. Kresse. 'Density functional study of CO on Rh(111)'. In: *Physical Review B* 70 (16 Oct. 2004), p. 165405. DOI: 10.1103/PhysRevB.70.165405 (cit. on p. 25).

[78] G. Henkelman, A. Arnaldsson and H. Jónsson. 'A fast and robust algorithm for Bader decomposition of charge density'. In: *Computational Materials Science* 36.3 (2006), pp. 354–360. DOI: 10.1016/j.commatsci.2005.04.010 (cit. on p. 26).

[79] W. Tang, S. Chill and W. Chai. *Bader Charge Analysis*. URL: https://theory.cm.utexas.edu/henkelman/research/bader/ (cit. on p. 26).

[80] A. P. J. Jansen. 'A Stochastic Model for the Description of Surface Reaction Systems'. In: *An Introduction to Kinetic Monte Carlo Simulations of Surface Reactions*. Berlin, Heidelberg: Springer Berlin Heidelberg, 2012, pp. 13–36. DOI: 10.1007/978-3-642-29488-4_2 (cit. on pp. 27, 28).

[81] G. N. Lewis. 'A New Principle of Equilibrium'. In: *Proceedings of the National Academy of Sciences* 11.3 (1925), pp. 179–183. DOI: 10.1073/pnas.11.3.179 (cit. on p. 28).

[82] M. Jørgensen and H. Grönbeck. 'MonteCoffee: A programmable kinetic Monte Carlo framework'. In: *Journal of Chemical Physics* 149.11 (2018). DOI: 10.1063/1.5046635 (cit. on p. 28).

[83] E. C. Dybeck, C. P. Plaisance and M. Neurock. 'Generalized Temporal Acceleration Scheme for Kinetic Monte Carlo Simulations of Surface Catalytic Processes by Scaling the Rates of Fast Reactions'. In: *Journal of Chemical Theory and Computation* 13.4 (2017), pp. 1525–1538. DOI: 10.1021/acs.jctc.6b00859 (cit. on p. 29).

[84] A. Chatterjee and A. F. Voter. 'Accurate acceleration of kinetic Monte Carlo simulations through the modification of rate constants'. In: *Journal of Chemical Physics* 132.19 (2010). DOI: 10.1063/1.3409606 (cit. on p. 29).

[85] K. A. Fichthorn and Y. Lin. 'A local superbasin kinetic Monte Carlo method'. In: *Journal of Chemical Physics* 138.16 (2013). DOI: 10.1063/1.4801869 (cit. on p. 29).

[86] M. G. Evans and M. Polanyi. 'Inertia and driving force of chemical reactions'. In: *Transactions of the Faraday Society* 34.0 (1938), pp. 11–24. DOI: 10.1039/TF9383400011 (cit. on p. 31).

[87] J. N. Bronsted. 'Acid and Basic Catalysis.' In: *Chemical Reviews* 5.3 (Oct. 1928), pp. 231–338. DOI: 10.1021/cr60019a001 (cit. on p. 31).

[88] F. Abild-Pedersen, F. Studt, J. Rossmeisl, R. J. Munter, P. G. Moses, E. Skulason, T. Bligaard, J. K. Nørskov and J. Greeley. 'Scaling Properties of Adsorption Energies for Hydrogen-Containing Molecules on Transition-Metal Surfaces'. In: *Physical review letters* 99.1 (2007), p. 0116105 (cit. on p. 31).

[89] R. A. van Santen, M. Neurock and S. G. Shetty. 'Reactivity Theory of Transition-Metal Surfaces: A BrønstedEvansPolanyi Linear Activation EnergyFree-Energy Analysis'. In: *Chemical Reviews* 110.4 (Apr. 2010), pp. 2005–2048. DOI: 10.1021/cr9001808 (cit. on p. 31).

[90] M. M. Montemore and J. W. Medlin. 'Scaling relations between adsorption energies for computational screening and design of catalysts'. In: *Catalysis Science & Technology* 4.11 (2014), pp. 3748–3761. DOI: 10.1039/C4CY00335G (cit. on p. 31).

[91] M. Anand and J. K. Nørskov. 'Scaling Relations in Homogeneous Catalysis: Analyzing the Buchwald–Hartwig Amination Reaction'. In: *ACS Catalysis* 10.1 (Jan. 2020), pp. 336–345. DOI: 10.1021/acscatal.9b04323 (cit. on p. 32).

[92] F. Calle-Vallejo, J. I. Martínez, J. M. García-Lastra, P. Sautet and D. Loffreda. 'Fast prediction of adsorption properties for platinum nanocatalysts with generalized coordination numbers'. In: *Angewandte Chemie - International Edition* 53.32 (2014), pp. 8316–8319. DOI: 10.1002/anie.201402958 (cit. on p. 32).

[93] F. Calle-Vallejo, D. Loffreda, M. T. M. Koper and P. Sautet. 'Introducing structural sensitivity into adsorption–energy scaling relations by means of coordination numbers'. In: *Nature Chemistry* 7.5 (2015), pp. 403–410. DOI: 10.1038/nchem.2226 (cit. on p. 32).

[94] F. Calle-Vallejo, J. Tymoczko, V. Colic, Q. H. Vu, M. D. Pohl, K. Morgenstern, D. Loffreda, P. Sautet, W. Schuhmann and A. S. Bandarenka. 'Finding optimal surface sites on heterogeneous catalysts by counting nearest neighbors'. In: *Science* 350.6257 (2015), pp. 185–189. DOI: 10.1126/science.aab3501 (cit. on p. 32).

[95] M. Jørgensen and H. Grönbeck. 'Scaling Relations and Kinetic Monte Carlo Simulations To Bridge the Materials Gap in Heterogeneous Catalysis'. In: *American chemical society* 7 (2017) (cit. on pp. 32, 34).

[96] J. L. C. Fajín, A. Bruix, M. N. D. S. Cordeiro, J. R. B. Gomes and F. Illas. 'Density functional theory model study of size and structure effects on water dissociation by platinum nanoparticles'. In: *The Journal of Chemical Physics* 137.3 (2012), p. 34701. DOI: 10.1063/1.4733984 (cit. on p. 35).

[97] Z. Cheng, N. A. Fine and C. S. Lo. 'Platinum Nanoclusters Exhibit Enhanced Catalytic Activity for Methane Dehydrogenation'. In: *Topics in Catalysis* 55.5 (2012), pp. 345–352. DOI: 10.1007/s11244-012-9803-5 (cit. on p. 35).

[98] N. K. Soliman. 'Factors affecting CO oxidation reaction over nanosized materials: A review'. In: *Journal of Materials Research and Technology* 8.2 (2019), pp. 2395–2407. DOI: 10.1016/j.jmrt.2018.12.012 (cit. on p. 35).

[99] R. Ducros and R. P. Merrill. 'The interaction of oxygen with Pt(110)'. In: *Surface Science* 55.1 (1976), pp. 227–245. DOI: 10.1016/0039-6028(76)90386-1 (cit. on p. 35).

[100] P. R. Norton, K. Griffiths and P. E. Bindner. 'Interaction of O2 with Pt(100). II. Kinetics and energetics'. In: *Surface Science* 138.1 (1984), pp. 125–147. DOI: 10.1016/0039-6028(84)90500-4 (cit. on p. 35).

[101] Y. Y. Yeo, L. Vattuone and D. A. King. 'Calorimetric heats for CO and oxygen adsorption and for the catalytic CO oxidation reaction on Pt{111}'. In: *Journal of Chemical Physics* 106.1 (1997), pp. 392–401. DOI: 10.1063/1.473203 (cit. on p. 35).

[102] K. McCrea, J. Parker and G. Somorjai. 'The Role of Carbon Deposition from CO Dissociation on Platinum Crystal Surfaces during Catalytic CO Oxidation: Effects on Turnover Rate, Ignition Temperature, and Vibrational Spectra'. In: *Journal of chemical physics* 106 (2002) (cit. on p. 37).

[103] K. McCrea, J. Parker and G. Somorjai. 'High-Pressure CO Dissociation and CO Oxidation Studies on Platinum Single Crystal Surfaces Using Sum Frequency Generation Surface Vibrational Spectroscopy'. In: *Surface Chemistry and Catalysis*. Ed. by Albert F Carley, Philip R Davies, Graham J Hutchings and Michael S Spencer. Boston, MA: Springer US, 2002, pp. 55–78. DOI: 10.1007/978-1-4757-6637-0_4 (cit. on p. 37).

[104] Y. O. Park, R. I. Masel and K. Stolt. 'An XPS study of carbon monoxide and nitric oxide adsorption on platinum (410): Unusual dissociation activity'. In: *Surface Science* 131.1 (1983), pp. L385–L389. DOI: https://doi.org/10.1016/0039-6028(83)90113-9 (cit. on pp. 38, 41).

[105] W. F. Banholzer, R. E. Parise and R. I. Masel. 'Adsorption and interaction of CO and NO on Pt(410): II. Infrared studies'. In: *Surface Science* 155.2 (1985), pp. 653–666. DOI: https://doi.org/10.1016/0039-6028(85)90020-2 (cit. on p. 38).

[106] J. M. Gohndrone, Y. O. Park and R. I. Masel. 'A comparison of nitric oxide decomposition on Pt(210) and Pt(410): An example where an increase in step density has produced a decrease in reactivity'. In: *Journal of Catalysis* 95.1 (1985), pp. 244–248. DOI: https://doi.org/10.1016/0021-9517(85)90024-7 (cit. on p. 38).

[107] S. Hagstrom, H. B. Lyon and G. A. Somorjai. 'Surface Structures on the Clean Platinum (100) Surface'. In: *Physical Review Letters* 15 (11 Sept. 1965), pp. 491–493. DOI: 10.1103/PhysRevLett.15.491 (cit. on p. 39).

[108] A. Borg, A.-M. Hilmen and E. Bergene. 'STM studies of clean, CO- and O2-exposed Pt(100)-hex-R0.7°'. In: *Surface Science* 306.1 (1994), pp. 10–20. DOI: https://doi.org/10.1016/0039-6028(94)91179-7 (cit. on p. 39).

[109] P. Heilmann, K. Heinz and K. Müller. 'The superstructures of the clean Pt(100) and Ir(100) surfaces'. In: *Surface Science* 83.2 (1979), pp. 487–497. DOI: https://doi.org/10.1016/0039-6028(79)90058-X (cit. on p. 39).

[110] J. Kullgren. 'Oxygen vacancy in ceria'. PhD thesis. Uppsala Universitet, 2012 (cit. on pp. 42, 44).

[111] Z. K. Han, Y. Z. Yang, B. Zhu, M. V. Ganduglia-Pirovano and Y. Gao. 'Unraveling the oxygen vacancy structures at the reduced Ce O2(111) surface'. In: *Physical Review Materials* 2.3 (2018), p. 35802. DOI: 10.1103/PhysRevMaterials.2.035802 (cit. on p. 43).

[112] M. V. Ganduglia-Pirovano, J. L. F. Da Silva and J. Sauer. 'Density-Functional Calculations of the Structure of Near-Surface Oxygen Vacancies and Electron Localization on CeO_2(111)'. In: *Physical Review Letters* 102 (2 Jan. 2009), p. 026101. DOI: 10.1103/PhysRevLett.102.026101 (cit. on p. 44).

[113] J. Carrasco, N. Lopez and F. Illas. 'First Principles Analysis of the Stability and Diffusion of Oxygen Vacancies in Metal Oxides'. In: *Physical Review Letters* 93 (22 Nov. 2004), p. 225502. DOI: 10.1103/PhysRevLett.93.225502 (cit. on p. 44).

[114] C. Barth, C. Laffon, R. Olbrich, A. Ranguis, Ph. Parent and M. Reichling. 'A perfectly stoichiometric and flat CeO2(111) surface on a bulk-like ceria film'. In: *Scientific Reports* 6.1 (2016), p. 21165. DOI: 10.1038/srep21165 (cit. on p. 44).

[115] P. M. Shah, J. W H Burnett, D. J Morgan, T. E Davies and S H Taylor. 'Ceria–Zirconia Mixed Metal Oxides Prepared via Mechanochemical Grinding of Carbonates for the Total Oxidation of Propane and Naphthalene'. In: *Catalysts* 9.5 (2019). DOI: 10.3390/catal9050475 (cit. on p. 44).

[116] T. Hasegawa, S. M. F. Shahed, Y. Sainoo, A. Beniya, N. Isomura, Y. Watanabe and T. Komeda. 'Epitaxial growth of CeO2(111) film on Ru(0001): Scanning tunneling microscopy (STM) and x-ray photoemission spectroscopy (XPS) study'. In: *Journal of Chemical Physics* 140.4 (2014). DOI: 10.1063/1.4849595 (cit. on p. 44).

[117] D. R. Mullins, S. H. Overbury and D. R. Huntley. 'Electron spectroscopy of single crystal and polycrystalline cerium oxide surfaces'. In: *Surface Science* 409.2 (1998), pp. 307–319. DOI: https://doi.org/10.1016/S0039-6028(98)00257-X (cit. on p. 44).

[118] M. S. Frei, C. Mondelli, R. García-Muelas, K. S. Kley, B. Puértolas, N. López, O. V. Safonova, J. A. Stewart, D. Curulla Ferré and J. Pérez-Ramírez. 'Atomic-scale engineering of indium oxide promotion by palladium for methanol production via CO2 hydrogenation'. In: *Nature Communications* 10.1 (2019), p. 3377. DOI: 10.1038/s41467-019-11349-9 (cit. on p. 44).

[119] A. Tovt, L. Bagolini, F. Dvořák, N. D. Tran, M. Vorokhta, K. Beranová, V. Johánek, M. Farnesi C., T. Skála, I. Matolínová, J. Mysliveček, S. Fabris and V. Matolín. 'Ultimate dispersion of metallic and ionic platinum on ceria'. In: *Journal of Materials Chemistry A* 7.21 (2019), pp. 13019–13028. DOI: 10.1039/c9ta00823c (cit. on p. 46).